Ph. D. DISSERTATION

WHITE QUANTUM DOT LIGHT-EMITTING DIODES BASED ON INVERTED DEVICE STRUCTURE

역구조 백색 양자점 발광다이오드 연구

BY

HEEYOUNG JUNG

FEBRUARY 2018

DEPARTMENT OF
ELECTRICAL AND COMPUTUER ENGINEERING
COLLEGE OF ENGINEERING
SEOUL NATIONAL UNIVERSITY

WHITE QUANTUM DOT LIGHT-EMITTING DIODES BASED ON INVERTED DEVICE STRUCTURE

역구조 백색 양자점 발광다이오드 연구

지도교수 이 창 희

이 논문을 공학박사 학위논문으로 제출함

2018 년 2 월

서울대학교 대학원

전기컴퓨터 공학부

정 희 영

정희영의 공학박사 학위논문을 인준함

2018 년 2 월

위 원 장 : _____ (인)
부위원장 : _____ (인)
위 원 : _____ (인)
위 원 : _____ (인)
위 원 : _____ (인)

Abstract

WHITE QUANTUM DOT LIGHT-EMITTING DIODES BASED ON INVERTED DEVICE STRUCTURE

HEEYOUNG JUNG
DEPARTMENT OF ELECTRICAL AND COMPUTER ENGINEERING
COLLEGE OF ENGINEERING
SEOUL NATIONAL UNIVERSITY

Colloidal quantum dots (QDs) have many advantages given their superior optical and electrical properties when used in optoelectronic devices. High photoluminescence quantum yields, broad absorption and narrow emission spectra, and stability with regard to thermal and optical stimuli make QDs excellent materials for light-emitting diodes (LED). After many years of research and advances in the development of materials and device engineering, quantum-dot light-emitting diodes (QLEDs) have undergone numerous improvements in terms of their performance capabilities and architectures. Among the possible applications,

white-light-emitting QLEDs have attracted significant attention due to the simplicity of their device architecture and the good flexibility of their emission spectrum. However, the charge carrier imbalance caused by the relatively large bandgap of blue QDs represents a hurdle preventing the achievement of high-performance white QLEDs. This thesis discusses the engineering of the hole transport layer (HTL) to control the hole injection rate into large-bandgap QDs and subsequent improvements in the device characteristics of white QLEDs.

I demonstrate an efficient blue QLED with a larger bandgap through HTL engineering. First, the influence of the highest occupied molecular orbital (HOMO) energy level in the HTL on the performance of QLEDs employing blue QDs with larger bandgaps is evaluated. Specifically, HTLs with various HOMO energy levels, *i.e.*, the CBP, mCP, TCTA, TAPC and NPB, are screened to investigate the device performance capabilities of blue QLEDs. Subsequently, CBP and mCP are chosen for use in the HTL of blue QLEDs. However, mCP when deposited onto the QD layer shows a non-uniform surface caused by a mismatch in the surface energy. Eventually, it was found that the co-deposition of CBP and mCP could successfully enhance the hole injection rate into blue QDs with larger bandgaps and could enable a uniform deposition on top of the QD layer. Blue QLEDs employing a CBP:mCP co-deposited layer exhibit a two-fold enhancement in the hole injection rates and thereby the luminescence efficiency.

A highly efficient and color-stable white QLED is then exhibited by implementing the CBP:mCP co-deposited layer. Red, green and blue primary-color QLEDs are fabricated with a CBP or a CBP:mCP co-deposited layer, after which all samples are characterized. Spectral changes and device efficiency rates with respect to the mixing ratio of the red, green and blue QDs are investigated. White QLEDs using a CBP or a CBP:mCP co-deposited layer are fabricated and the relationships

between the enhancement of each primary-color QLED and that of white QLEDs are investigated. The co-deposition of CBP and mCP allows a two-fold enhancement of the hole injection rate into the large-bandgap QDs, resulting in a considerable enhancement of the device performance in terms of the luminescence efficiency and the operational stability of corresponding QLEDs. Furthermore, the co-deposited HTL reduces the driving voltage of the large-bandgap QDs and subsequently improves the color stability of white QLEDs for improved temporal and operational dependency. The resulting white QLEDs emit white-emission around an equal energy point in the Commission Internationale de l'Eclairage 1931 chromaticity diagram and exhibit an external quantum efficiency rate exceeding 5 % at brightness levels ranging from 100 to 10,000 cdm^{-2}.

I believe that the suggested device architecture and the technological guideline presented in this thesis will be helpful to those developing efficient and color-stable white QLEDs.

Keywords: Colloidal Quantum Dot, Light-Emitting Diodes, Inverted Structures, Co-deposition, Hole Transport Layer, Charge Injection Balance

Student Number: 2012-20866

Contents

List of Figures

List of Tables

Chapter 1

Introduction

1.1 Colloidal Quantum Dot Light-Emitting Diodes

Colloidal quantum dot (QD) has attracted significant attention as a promising illuminant since it discovered by Alexey Ekimov [1] and Louis Brus [2] in early 1980's. QDs have several unique characteristics, wide absorption, narrow emission spectra, tunable emission wavelength by composition and size controlling, and solution processability [3-9]. These properties make QDs adoptable to multiple applications like light-emitting diodes (LEDs) [10-13], color filter [14-17], solar cell [18-20], luminescence solar concentrators [21-24], bioimaging [25-27], et cetera. Especially, QDs are promising lumophors for LEDs. These are many advantages of Quantum dot light-emitting diodes (QLEDs) s for application to display. First, QDs shows narrow emission spectra. Organic dyes have tails in spectra due to vibronic states, but QDs have very narrow emission spectra with gaussian shape. Narrow

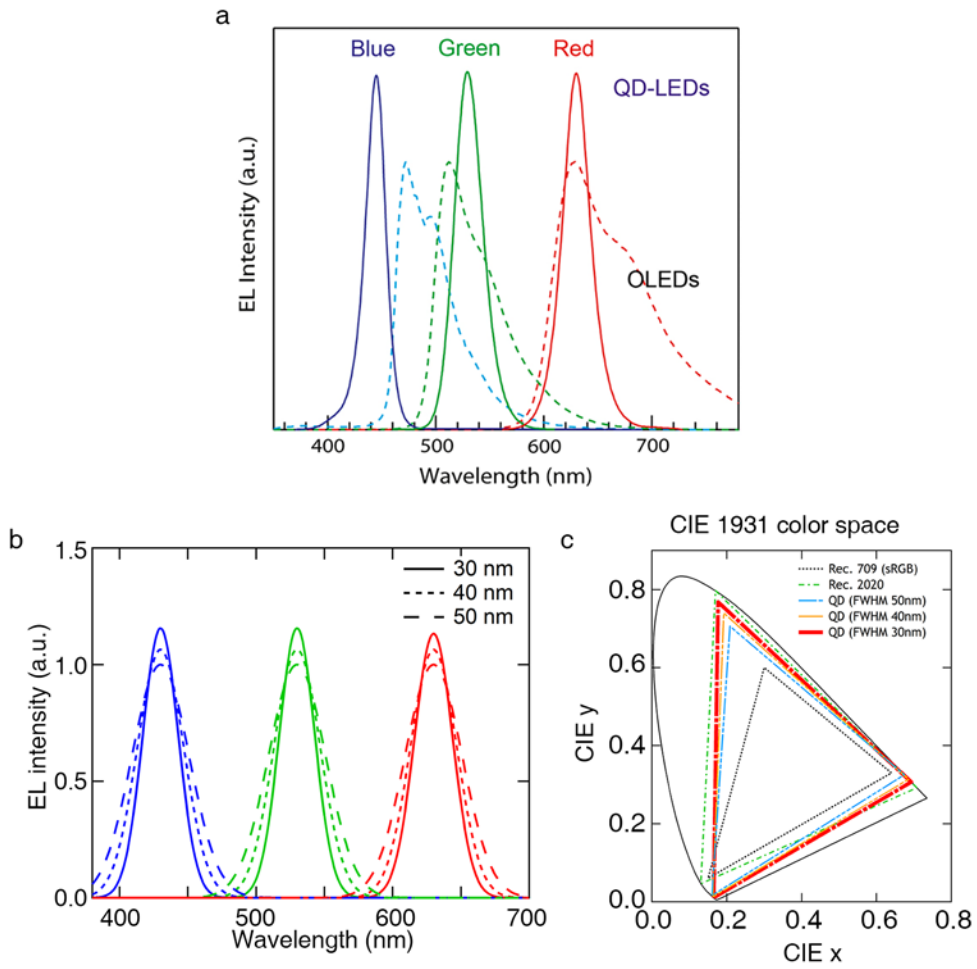

Figure 1.1 (a) Comparison of red, green and blue EL spectra with (dashed lines) OLEDs and (solid lines) QLEDs. (The figure is taken from reference [8]) (b) The spectrum of red, green and blue QDs depending on the FWHM range from 30 nm to 50 nm. (c) The CIE (Commission Internationale de l'Eclairage) 1931 chromaticity diagram of theoretical QDs emitting 430, 530, and 630 nm with 30 nm (red line), 40 nm (orange line) or 50 nm (blue line) of FWHM. Rec. 2020 (green line) and Rec. 09 (black line) color gamut are also illustrated. The emission spectra of QDs are assumed as Gaussian shape.

emission bandwidth guarantees high color purity and wide area in Color Gamut, compared to liquid crystal display (LCD) and organic light-emitting diodes (OLED) display. Despite rapid advances in the technologies and expansion in the display market of OLEDs, the broad width of the electroluminescence (EL) emission band is a drawback of the OLED technology. Full-width at half-maximum (FWHM) of OLEDs is greater than 40 nm due to the vibronic states of organics dyes. On the other hand, FWHM of QLEDs employing cadmium (Cd)-based QD emitter is similar or less than 30 nm. Figure 1.1a shows that the EL spectra of typical OLEDs is broader than the Cd-based QLEDs. Narrow bandwidth of QD emitter widen the color reproducible range of QLEDs in the color gamut. As each FWHM of red-, green- and blue-QD are smaller, represented color reproducible range of QLEDs becomes wider and closes to the Rec.2020 in the color gamut (Figure 1.1b). Thanks to the superior color reproducibility of QDs, global TV suppliers such as Samsung Electronics, LG Electronics, TCL Corporation and Sony had released the TV display employing QDs in the global market (Figure 1.2). Color conversion films consist of polymer matrix and QDs attached in front of back-light unit (BLU) of LCD. High photoluminescence quantum yield (PLQY) and small FWHM allow LED TV using QD color conversion film to be more vivid and bright than that using phosphor color converter. Second, QDs have bandgap tunability in terms of engineering core size and core composition of QDs. Core size of QD decides center wavelength of emission spectra. So it is possible to realize QLEDs that emits various color range including infrared (IR), visible, ultraviolet (UV). Finally, QLEDs shares the structure and material with OLEDs. QLEDs have composed of anode, hole injection layer (HIL), hole transport layer (HTL), QD emissive layer, electron transport layer (ETL), electron injection layer (HIL) and cathode electrode. This makes QLEDs adopt pre-developed charge transport materials (CTMs) in OLED fields as efficient

charge transport layer (CTL) of QLEDs. Various CTMs developed in OLED field and device operation mechanism elucidated by researcher working in OLED field helps the evolution of inorganic-organic hybrids types QLEDs. Luminescence and device efficiency of QLEDs are increased steeply. Outstanding optoelectronic properties of QDs and rapid development of QLEDs guarantee that QLEDs would be the rising EL devices for the next generation display.

Figure 1.2 Display application of QDs

The research trend of QLEDs is shown in figure 1.3. The first QLED was developed in 1994 [28]. V.L Colin *et al.* fabricated the QLEDs that had simple structure of indium tin oxide (ITO)/poly(p-paraphenylene vinylene) (PPV)/CdSe QDs/Mg. The device performance in terms of a maximum luminosity of 100 cdm^{-2} and an external quantum efficiency (E.Q.E.) of 0.001-0.01 % is not sufficiently enough to distinguish the emission from QDs and nearby PPV organic layer. Few years later, a device efficiency of QLEDs was increased significantly with adopting a multilayer structure by S. Coe *et al* [29]. They used the N,N'-diphenyl-N,N'-bis(3-methylphenyl)-1,1'-biphenyl)-4,4' -diamine (TPD) as HTL and tris-(8-hydroxyquinoline) aluminium (Alq3) as ETL. Insulting HTL and ETL to QLEDs enabled the efficient charge injection into QDs emissive layer and isolate the luminescence process from charge conduction. As a results, they obtained the device efficiency of 0.52 % E.Q.E. Although they fabricated multilayer QLEDs, there were still an issue for fabrication. Because the solvent of QDs dissolved the underlying organic HTL during solution process deposition, they used the phase separation method. Organic hole transport material (HTM) and QDs were dissolved in same solution then spin-casted at the same time. But phase separation method could not make the perfect bilayer structure, so they observed the aggregation of QDs onto TPD layer by morphological analysis. Q.-J Sun *et al.* introduced the cross linkable HTL to QLEDs, that allows spin-casting QD layer without any damage to below cross linked HTL [30]. The solvent robust of cross linked HTL allows uniform spin-coating of QDs on top of organic HTL and resulting devices shows brightness over 9,000 cdm^{-2}. Studies about the functional ligands attached to QDs started to give them the unique properties that helps QLEDs overcome the problems likes uniform film formation, balanced carrier transporting [31, 32]. For many years, carrier injection, especially the hole injection to QD is barrier to obtain high performance

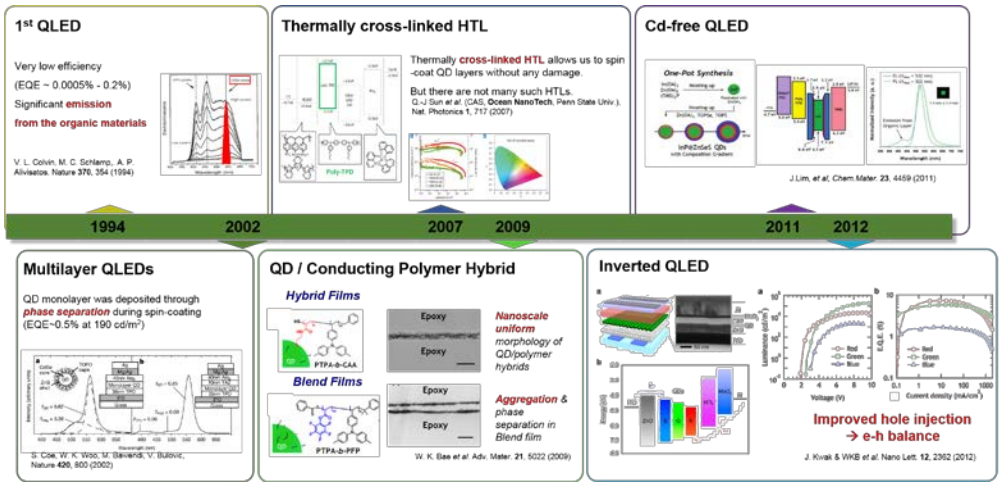

Figure 1.3 Research trends of QLEDs. The first development of QLED, multi-layered QLEDs, QLEDs employing cross-linkable HTL, research on functional ligand, cd-free QLED and development of inverted structure are illustrated..

QD optoelectronic devices. The difference between high valence band edge (VBE) energy level of inorganic QDs (~ 7 eV) and highest occupied molecular orbital (HOMO) energy acts of HTM (5-6 eV) as the energetic barrier to inject hole from HTL into QD emissive layer. Screening various HTMs to reduce the hole injection barrier of QLED is limited by the solution process orthogonality. HTMs has to stand against the solution process deposition of QDs. J. Kwak *et al.* introduced an inverted structure QLEDs [33]. The inverted structure QLEDs enabled varied small molecule materials available for the HTL of the QLEDs. This inverted system facilitates HOMO energy level engineering by employing variety of organic HTLs with different HOMO energy levels processed by thermal evaporation onto solution processed QDs. The performance of the QLEDs increased dramatically by the HOMO level engineering of the HTLs. To avoid environmental issues and industrial restrictions caused by using Cd-based material, QLEDs implanting Cd-free QDs

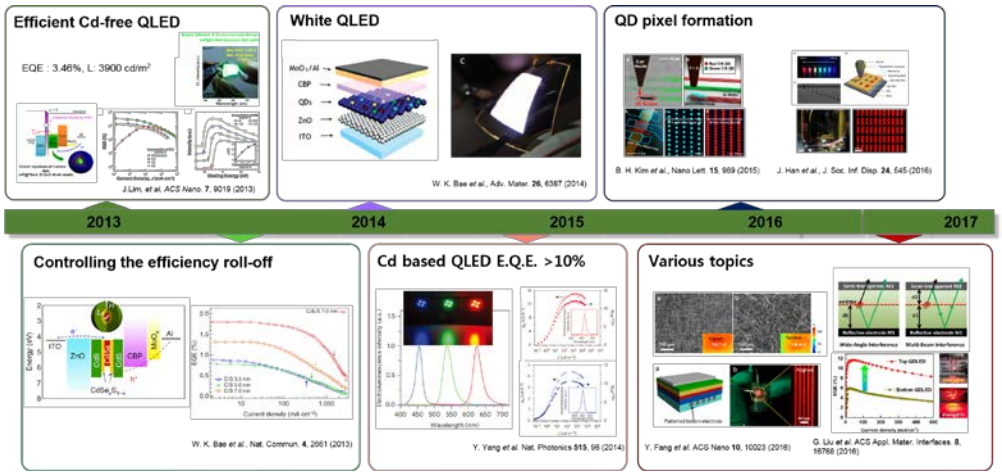

Figure 1.4 Research trends of QLEDs. Cd-free QLEDs with inverted structure, studies on efficiency roll-off, white QLEDs, high performance QLEDs, pixilation of QLEDs and researches for applications are described.

were developed and studied. InP QDs [34-36], CuInS (CIS) QDs [37-39] or Mn doped ZnSe QDs [21, 40, 41] were suggested to substitute for Cd-based QDs. Device performance of Cd-free QLEDs were improved by adopting techniques researched in Cd-based QLEDs fields and modulating core/shell structure of Cd-free QD but still below the performance of Cd-based QLEDs[36]. Other limitations of QLEDs like efficiency roll-off due to charge imbalance, the auger recombination and energy transfer between QDs are studied [42, 43]. High performance white QLEDs are realized by just mixing the red, green, and blue QDs in single layer [10, 11, 44]. Nowadays, primary color of red-, green- and blue-QLEDs exceed over 10 % E.Q.E. [45] and red QLEDs are reached 21 % E.Q.E. [46]. QDs start to be used in commercial applications especially in display so that researchers are interested in QLEDs for real applications, *i.e.* high resolution patterning [47-49], flexible and transparent display [50] or extremely high efficiency using out coupling effect [51].

1.2 White Quantum Dot Light-Emitting Diodes

White luminescence sources have been developed for a long history due to their importance in human society. White light emission is most important role of EL devices for its potential applications to BLU of LCD, LEDs or lighting sources. As a white luminescence source, white-QLEDs have remarkably attractive properties and functionalities. Every single QD has inherent color spectra decided by the core composition and core size. Overlap of individual QDs that have difference color generates white emission spectra. In the same way, mixed colored QD layer in QLEDs produces white light emission. White-QLEDs could be fabricated in the same way with the single colored QLEDs and spectrum of white emission could be simply adjustable by mixing QDs with requisite spectrum. Due to the simplicity in the device architecture and flexibility in the emission spectrum, white-QLEDs have attracted great attention as next generation solid state light source for display [46, 52, 53] and lighting [12, 54] applications.

There were efforts to succeed QDs to phosphor of white LEDs owing to superior optical characteristics of QDs such as high PLQY, narrow emission spectra and bandgap tunability as well as robust material characteristics of QDs such as high photo stability [55] and thermal stability [56, 57]. Red and green QDs were dispersed in epoxy resin. QDs dispersed resin were integrated with inorganic LED and QDs converted blue light of inorganic LED to red and green light with narrow band linewidth [14, 58]. Surrounding resin passivated QDs from external harsh atmosphere and protected QDs during packing process. Simple process, high robustness, excellent PLQY, superior color reproducibility and compatibility with conventional display technologies have made QD color converter commercially viable prior to QLEDs display.

Figure 1.5 Various applications of white QLEDs (The image is taken from reference [11]).

Successive development of materials and device structure for white QLEDs allows dramatic improvements of white QLEDs in device efficiency and color purity. The first white QLEDs with mixed colored QDs developed by P. O. Anikeeva *et al.* exhibited 0.36 % E.Q.E. [10]. The PLQY of primary color QDs have been improved and suitable device architecture and CTLs have been developed to reduce the energetic barrier for balanced carrier injection. As a results, E.Q.E. of white-QLEDs exceeds 10 % these day [44]. In 2014, W. K. Bae et al. reported white-QLEDs that showed dichromatic, trichromatic and tetrachromatic white color [11]. Individual QDs with red, yellow, green, cyan and blue color were synthesized and mixed for fabricating dichromatic, trichromatic or tetrachromatic white-QLEDs. Dichromatic white-QLEDs consisted of blue and yellow QDs realized white light using simple double colored QDs and clear red, green and blue light could be obtained by filtering white light emitted from trichromatic white-QLEDs through red, green and blue color filter. White light with excellent color rendering index (CRI) over 93 emitted by tetrachromatic white-QLEDs appropriated for reproducing daylight illumination.

Despite these improvement of white-QLEDs, device performance of white-QLEDs still far from real display application. Relatively large band gap of blue-QDs compared to red- or green-QDs in the white-QLEDs prevents efficient hole injection

from HTL into blue-QDs. Mixing large number fraction of blue-QDs for emissive layer of white-QLEDs is inevitable owing to the relatively low efficiency of blue-QLEDs as well as the energy transfer from blue QD to smaller bandgap red and green QD [59-61]. The device efficiency of white-QLEDs is largely affected by blue-QDs that have large portion in red-, green- and blue-QDs mixture. Key issue for improving the efficiency of white-QLEDs is enhancing device performance of blue-QLEDs by reducing charge injection imbalance and thereby the device performance of white-QLEDs.

Table 1.1 Performance parameters of white QLEDs using single layer of red, green and blue QDs.

Peak w of red QDs (nm)	Peak w of green QDs (nm)	Peak w of blue QDs (nm)	Max E.Q.E. (%)	Max C.E. (cd/A)	Max P.E. (lm/W)	Max luminance (cd/m^2)	CIE x	CIE y	Ref.
624	545	453	1.3		2.4	6400	0.34	0.36	[11]
611	520	448	10.9	21.8		23352	0.22	0.188	[44]
611	520	448					0.317	0.325	[44]
620	540	440	0.36	0.9	0.57	830	0.35	0.41	[10]
618	539	499		0.4			0.37	0.45	[90]
640	520	440	0.6			3000			[91]
640	520	440	1.6			4000	0.39	0.38	[91]

1.3 Outline of Thesis

This thesis consists of five chapters, including the Introduction and Conclusion. As an introduction, Chapter 1 describes the previous research on colloidal QLEDs and the advantages of white QLEDs and key issues for improving white QLED. Chapter 2 includes the methods for preparing materials: the methods used to prepare ZnO nanoparticles; the highly luminescent type I red, green and blue heterostructured QDs; and the organic materials used in this thesis are described in detail. In addition, the fabrication and characterization methods for the QLED devices are summarized in this chapter, and the electrical and morphological characterization methods for thin films used in this thesis are depicted. Characterization methods for electrical and morphological characteristics of thin films are also described in this Chapter. In Chapter 3, the influence of HOMO energy level of HTL on the performance of QLEDs employing larger-bandgap blue-QDs is evaluated. The HTL of 4,4'-bis(carbazol-9-yl)biphenyl (CBP), 1,3-Bis(N-carbazolyl)benzene (mCP), 4,4',4''-tris(N-carbazolyl)-triphenylamine (TCTA), 4,4'-Cyclohexylidenebis[N,N-bis(4-methylphenyl)benzenamine] (TAPC) and N,N'-Di(1-naphthyl)-N,N'-diphenyl-(1,1'-biphenyl)-4,4'-diamine (NPB) are screened to investigate the efficiency and turn-on voltage of blue-QLEDs. Then we found that higher HOMO energy level of HTL leads to the enhanced device performance except for the case of mCP. We analyzed the morphologies of CBP and mCP on the QD layer. Surface energy mismatch between mCP and QD layer leads to the uneven surface of mCP layer on QD layer and short current path. Then we devised the CBP:mCP co-deposited layer that modified the surface energy of mCP and formed the uniform surface on QD layer. Blue-QLEDs employing CBP:mCP co-deposited layer have been fabricated and investigated. Proposed device displays enhanced hole

injection rates and thereby the luminescence efficiency owing to the higher LUMO energy level and hole density of CBP:mCP co-deposited layer In Chapter 4, suggested architecture in previous Chapter is applied to the white QLED. Red, green and blue primary colored QLEDs are fabricated with CBP or CBP:mCP co-deposited layer then characterized. Spectral changes and device efficiency with respect to the mixing ratio of red, green and blue QD are investigated. White QLEDs using CBP or CBP:mCP co-deposited layer are fabricated and the relationship between the enhancement of each primary colored QLEDs and that of white QLEDs are investigated. We found that the ratios in EL increment in red, green and blue of white-emission resulting from employment of CBP:mCP co-deposition layer agree well with E.Q.E. increment of red, green and blue emitting primary color QLEDs. The color stabilities along with the temporal dependency and operational dependency are investigated. White QLEDs employing CBP:mCP co-deposited layer exhibits superior stability characteristics. Finally, in Chapter 5, we summarize our work and present concluding remarks.

Chapter 2

Experimental Methods

2.1 Materials

2.1.1 Preparation of ZnO Nanoparticles

ZnO nanoparticles were synthesized modifying the method reported by Pacholski *et al.* At first, 1.23 g of $Zn(Ac)_2 \cdot 2H_2O$ was dissolved in 55 ml of methanol at room temperature. Then, 25 ml of a methanol solution containing 0.48 g of KOH was added dropwise at 60 ºC with magnetic stirring. The reaction mixture was kept at 60 ºC for 2 h under N_2 atmosphere. The product appeared as white precipitate. After collecting by centrifugation, this white precipitate was washed with methanol. Finally, 0.1 ml of butylamine was added for stabilization and the precipitate was redispersed in butanol (20 $mgml^{-1}$).

2.1.2 Synthesis of Red-color Emitting CdSe(core radius (r) = 2.0 nm)/$Zn_{1-X}Cd_XS$(shell thickness (h) = 6.0 nm) Core/shell Heterostructured Quantum Dots

Chemicals: Cadmium oxide (CdO, 99.9%), zinc oxide (99.9%), selenium (200 mesh, 99.999%), 1-dodecanethiol (DDT, 98%), tri-*n*-octylphosphine (TOP, 90%), myristic acid (MA, 90%) were purchased from Alfa Aesar. Sulfur (99.9%), oleic acid (OA, technical grade) and 1-octadecene (ODE, 90%) were obtained from Sigma Aldrich. General organic solvents were acquired from Daejung (Korea). All chemicals were used as received without further purification.

Synthesis of CdSe/$Zn_{1-X}Cd_XS$ QDs: QD synthesis was preceded with the Schlenk line technique under inert conditions. The cationic precursors (0.5 M cadmium oleate ($Cd(OA)_2$) and 0.5 M zinc oleate ($Zn(OA)_2$)) were prepared by dissolving the 100 mmol of CdO and ZnO in mixed solvent of 100 ml of OA and 100 ml of ODE (total volume 200 ml) under N_2 at 300 °C for 1hr. The anionic precursors (2 M TOPSe and 2 M TOPS) were made by dissolving 20 mmol of selenium and sulfur in 10 ml of TOPSe under N_2 at 100 °C for 1hr. For CdSe/$Zn_{1-X}Cd_XS$ (r = 2.0 nm, R = 4.5 nm), 1 mmol of CdO, 3 mmol of MA and 15 ml of ODE were loaded in 3 neck flask and heated up to 300 °C under the inert conditions to form $Cd(MA)_2$ complex. After reactants were turned to be optically clear, 0.25 ml of 2 M TOPSe was rapidly injected into the reaction flask to form CdSe core. After 3 min of reaction, 3 ml of 0.5 M $Zn(OA)_2$ precursor and 1 mmol of DDT were added drop wisely within 1 min. The reaction was preceded for 30 min to yield $Zn_{0.4}Cd_{0.6}S$ inner shell. 2 ml of 0.5 M $Cd(OA)_2$, 4 ml of 0.5 M $Zn(OA)_2$ and 1.5 ml of 2 M

TOPS were added into the reaction flask within 1 min for $Zn_{0.5}Cd_{0.5}S$ shelling and the reaction was proceeded for 10 min. The repeated precursor injection yielded the successive growth of $Zn_{0.5}Cd_{0.5}S$ outer shell growth. Synthesized QDs were purified 10 times by the precipitation/redispersion (ethanol/toluene) method. Final products were dispersed in hexane at a concentration of 20 $mgml^{-1}$.

2.1.3 Synthesis of Green-Color Emitting $Cd_{1-X}Zn_XSe$(r = 1.5 nm)/ZnS(h = 6.2 nm) Core/shell Heterostructured Quantum Dots

Chemicals: Cadmium oxide (CdO, 99.95%, metals basis), selenium (Se, 99.99%) and myristic acid (MA, ≥ 99%) were purchased from Alfa Aesar. Zinc acetate ($Zn(Ac)_2$, 99.99%, metals basis), 1-octadecene (ODE, 90%), sulfur (S, 99.998%), oleic acid (OA, technical grade 90%), 1-dodecanethiol (DDT, ≥ 98%) and tri-n-octylphosphine (TOP, ≥ 99%) were purchased from UniAm (Korea). Zinc acetate dihydrate ($Zn(Ac)_2{\cdot}2H_2O$, ≥ 98 %), Potassium hydroxide (KOH, Reagent grade, 90%) and butylamine (99.5%) was obtained from Sigma-Aldrich. Organic solvents were obtained from Sigma-Aldrich and used as purchased. 4,4'-Bis(N-carbazolyl)-1,1'-biphenyl (CBP, > 99.9 %) and 1,3-Bis(N-carbazolyl)benzene (mCP, > 99.9 %) were purchased from OSM (Korea).

Preparation of stock solutions: We prepared the stock solutions [0.5 M cadmium oleate ($Cd(OA)_2$), 0.5 M zinc oleate ($Zn(OA)_2$), 2M selenium dissolved in tri-n-octylphosphine (TOPSe), 2M sulfur dissolved in tri-n-octylphosphine (TOPS) and 0.5M sulfur dissolved in ODE (SODE)]. 50 mmol of CdO (or $Zn(Ac)_2$) in a mixed solution of 50 ml of OA and 50 ml of ODE were degassed at 110 ^oC for 2 h.

The reaction flask was back-filled with Ar, then heated up to 240 ^{o}C for 1 h, degassed again at 110 ^{o}C. 2M TOPSe and TOPS were prepared by dissolving 60 mmol of selenium and sulfur powder in 30 ml of TOP at 100 ^{o}C for 1 h under Ar atmosphere. 0.5 M SODE precursor was prepared by dissolving 10 mmol of sulfur powder in 20 ml ODE at 100 ^{o}C under Ar atmosphere.

Synthesis of $Cd_{1-X}Zn_XSe/ZnS$ green QDs: As a typical synthetic procedure, 0.4 mmol of CdO, 4 mmol of Zn $(Ac)_2$, 17.6 mmol of OA, and 20 mL of ODE were placed in a 100 ml round flask. The mixture was heated to 150 °C, degassed for 30 min, and back-filled with Ar gas. The reaction flask heated up to 300 °C to form a clear solution of $Cd(OA)_2$ and $Zn(OA)_2$. At this temperature, 0.4 mmol of TOPSe and 4 mmol of TOPS mixture were quickly injected into the reaction flask. After the injection, the reaction was preceded for 10 min to form a CdZnSe core and 4 mmol of $Zn(OA)_2$ and 4 mmol of TOPS was injected drop wisely within 10 min. After 10 min of reaction, QDs were purified by adding 20 ml of toluene and an excess amount of ethanol (5 times); they were then redispersed in toluene at a concentration of 30 $mgml^{-1}$.

2.1.4 Synthesis of Blue-color Emitting $Cd_{1-X}Zn_XS$(r = 2 nm)/ZnS(h = 2.3 nm) Quantum Dots

As a synthetic procedure, 1 mM of CdO, 10 mM of $Zn(acet)_2$, 7 mM of OA were placed in a 100 mL round flask. The mixture was heated to 150 °C, degassed under 100 mTorr pressure for 20 minutes, filled with N_2 gas, added with 15 ml of 1-ODE and further heated to 300 °C to form a clear solution of $Cd(OA)_2$ and $Zn(OA)_2$. At this temperature, 2 mM of S powder dissolved in 3 mL of 1-ODE were quickly

injected into the reaction flask. After the first injection of S precursors, the temperature of the reaction flask was elevated to 310 °C for further growth of $Cd_{1-x}Zn_xS$ cores. After the elapse of 8 min of reaction, 8 mM of S powder dissolved in tributylphosphine (TBP, 90 %) were introduced into the reactor to overcoat existing $Cd_{1-x}Zn_xS$ cores with ZnS shells without any purification steps. Aliquots of QDs were taken during the reaction to analyze the development of QDs. After the reaction was completed, the temperature was cooled down to room temperature. QDs were extracted and purified by adding 20 ml of chloroform and an excess amount of acetone (done twice); then they were redispersed in chloroform or hexane for further characterization. In order to adjust the optical properties of QDs, the amount of S precursors in the first injection was varied maintaining the other entire parameters constant.

2.1.5 Organic Materials

4,4'-bis(carbazol-9-yl)biphenyl (CBP), 1,3-Bis(N-carbazolyl)benzene (mCP), 4,4',4''-tris(N-carbazolyl)-triphenylamine (TCTA), 4,4'-Cyclohexylidenebis[N,N-bis(4-methylphenyl)benzenamine] (TAPC) and N,N'-Di(1-naphthyl)-N,N'-diphenyl-(1,1'-biphenyl)-4,4'-diamine (NPB) are purchased from OSM as hole transport layer. Chemical structures of organic materials used in this thesis are as follows.

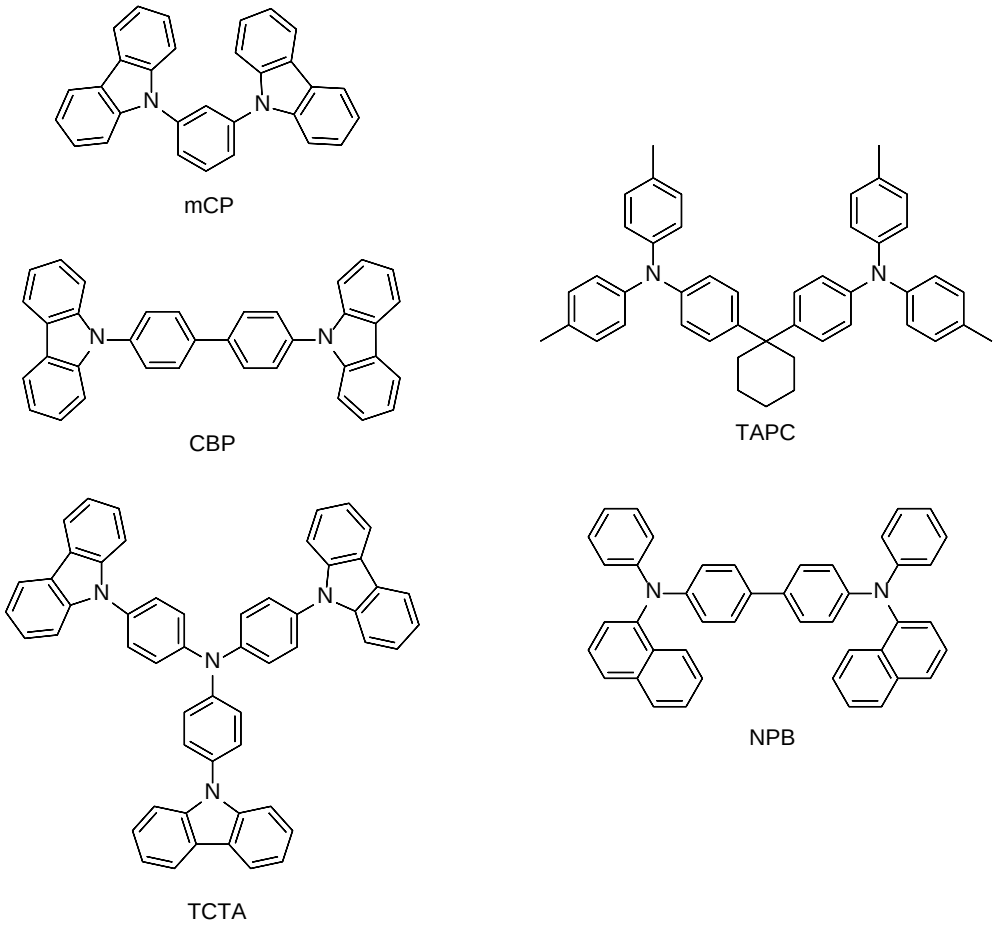

Figure 2.1 Chemical structures of CBP, mCP, TCTA, TAPC and NPB.

2.2 Device Fabrication and Characterization Methods

2.2.1 Device Fabrication

All QLED devices were basically fabricated using the inverted structures and the detail structures, materials and processes are introduced in each chapter. First of all, patterned ITO glass substrates were prepared, which were cleaned with acetone, isopropanol and deionized water in an ultrasonicator (Branson 5510). And then the cleaned ITO glass substrates were dried in the oven at 120 °C. For the inverted structure, 20 mg/mL of the ZnO nanoparticle solution was spin-coated on a patterned ITO glass with a spin-rate of 2000 rpm for 60 sec and dried at 90 °C for 30 min in the oven filled with N_2 gas. The thickness of ZnO layer as electron injection/transport layer was about 45 nm. QD solution was spun on the bottom layer at 4000 rpm for 30 sec, followed by baking in N_2 oven at a temperature of 70 °C. Then HTLs (NPB, TAPC, TCTA, CBP, mCP or CBP:mCP (1:1) co-deposited layer), MoO_x, and Al electrode were thermally evaporated under a vapor pressure of 1×10^{-6} torr onto QDs coated substrates. The deposition rates of each layers were 1 $Å s^{-1}$ for NPB, TAPC, TCTA, CBP or mCP sole layer. CBP and mCP were evaporated with deposition rates of 0.5 $Å s^{-1}$ simultaneously for CBP:mCP (1:1) co-deposited layer. And then MoO_x, and Al were thermally evaporated with rate of 0.2 $Å s^{-1}$, and 4–5 $Å s^{-1}$, respectively.

2.2.2 Current-voltage-luminance Measurement

The current-voltage (I-V) characteristics were measured with a Keithley 236 source measurement unit, while the electroluminescence was measured with a calibrated Si photodiode (Hamamatsu, S5227-1010BQ) with a size of 10 mm × 10 mm placed at an angle normal to the device surface, assuming that the device was a Lambertian source. To detect a turn-on voltage of light-emitting diodes, we use an ARC PD438 photomultiplier tube (PMT) with the Keithley 236 source measurement unit. The electroluminescence (EL) spectra and the Commission Internationale de L'Eclairage (CIE) color coordinates were measured with a Konica-Minolta CS-1000A spectroradiometer. The luminance and efficiency were calculated from the photocurrent signal of photodiode with a Keithley 2000 multimeter, and corrected precisely with the luminance from spectroradiometer (CS-2000).

The chromatic characteristics were calculated from EL spectra measured by the CS-1000A spectrometer using the CIE 1931 color expression system. The tristimulus values XYZ can be calculated by following equations,

$$X = K_m \int_0^\infty \bar{x}(\lambda) P(\lambda) d\lambda \tag{2.1}$$

$$Y = K_m \int_0^\infty \bar{y}(\lambda) P(\lambda) d\lambda \tag{2.2}$$

$$Z = K_m \int_0^\infty \bar{z}(\lambda) P(\lambda) d\lambda \tag{2.3}$$

where, P(λ) is a given spectral power distribution of emissive source, $\bar{x}$, $\bar{y}$ and $\bar{z}$ are the CIE standard color matching functions (see Figure 2.2) and Km is the weighing constant (683 lm W^{-1}). From the tristimulus values, the CIE color coordinates calculated by following equations,

$$x = \frac{X}{X+Y+Z} \tag{2.4}$$

$$y = \frac{Y}{X+Y+Z} \tag{2.5}$$

$$z = \frac{Z}{X+Y+Z} \tag{2.6}$$

Any color can be plotted on the CIE chromaticity diagram.

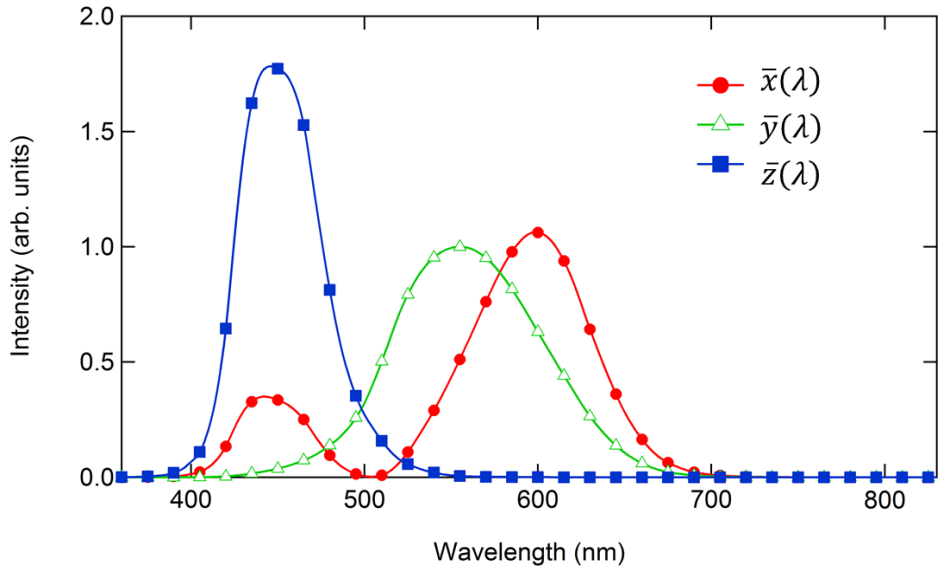

Figure 2.2 The CIE standard observer color matching functions

2.2.3 Efficiency Calculation Methods

To evaluate the emission properties of light-emitting diodes, the commonly employed efficiencies are the external quantum efficiency (E.Q.E.), the current efficiency (C.E.) and the power efficiency (P.E.).

The external quantum efficiency can be defined by the following equation.

$$\text{E. Q. E.} = \frac{number\ of\ emitted\ photons}{number\ of\ injected\ electrons}(\%)$$

Typically, QLEDs or OLEDs emit light into the half plane due to the metal contact. Without any modification for increasing out-coupling efficiency, over 80% of the emission can be lost to internal absorption and wave-guiding in a simple planar light-emitting device.

Since human eye has different spectral sensitivity in visible area, the response of the eye is standardized by the CIE in 1924 (see $\bar{y}$ in Figure 2.2). The luminous efficiency weighs all emitted photons according to the photopic response of human eye. The difference is that E.Q.E. weighs all emitted photons equally. C.E. can be expressed by the following equation.

$$\text{C. E.} = \frac{luminance}{current\ density}(cd\ A^{-1})$$

The luminance value (cd m^{-2}) can be easily measured by the commercial luminance meter (CS-1000A in this thesis).

The power efficiency is the ratio of the lumen output to the input electrical power as follows,

$$\text{P. E.} = \frac{luminous\ flux}{electrical\ power}(lm\ W^{-1})$$

The E.Q.E.s can be useful to understand the fundamental physics for light emission mechanism, while the PEs can be useful to interpret the power dissipated in a light-emitting device when used in a display application.

2.2.4 Measurement of electrical characteristics of thin films

Device fabrication and characterization of hole only device (HOD): HOD with CBP, mCP or CBP:mCP co-deposition HTL were fabricated and characterized to obtain the conductivity, hole density and impedance of HTLs. Indium tin oxide (ITO) patterned glass was cleaned with acetone, isopropyl alcohol, and deionized water sequentially and then used as substrate for HOD. The prepared Poly(3,4'-ethylenedioxythiophene)-poly(styrenesulfonate) (PEODT:PSS) solution was spun-cast on patterned ITO substrates with a spin rate of 4000 rpm for 60 s. PEDOT:PSS films were then annealed at 120 °C under 100 mtorr pressure for 30 min. Then HTLs (CBP, mCP or CBP:mCP (1:1) co-deposited layer), MoO_x, and Al electrode were thermally evaporated under a vapor pressure of 1×10^{-6} torr. Transient characteristics were measured by using oscilloscope (MDO4000) and the current density–voltage (*J–V*) characteristics were measured by using Keithley-236 source measurement unit using the closed cycle cryostat for temperature variation of the sample. The frequency dependent measurements were performed with impedance analyzer (Wayne Kerr 6500B). The relationship

$$\sigma = p \times e \times \mu,$$

relating conductivity (σ), mobility (μ), and carrier density is used to calculate the hole density (p), where e is 1.602×10^{-19}C.

Device fabrication and characterization of metal-insulator-semiconductor (MIS) diodes: MIS diodes with CBP or CBP:mCP co-deposition HTL were fabricated and characterized to obtain the mobility of HTLs. For preparing Ta_2O_5 sol-gel solution, 0.65 ml of tantalum ethoxide ($Ta(OC_2H_5)_5$) and 0.14 ml of acetic acid was dissolved in 5 ml of ethanol at room temperature[S5]. Then the Ta_2O_5 sol-gel solution was stirred overnight. Then prepared Ta_2O_5 sol-gel solution was spun-cast on patterned ITO substrates with a spin rate of 8000 rpm for 40 s. Ta_2O_5 sol-gel films were then annealed at 400 °C for 1 hour. Then HTLs (CBP or CBP:mCP (1:1) co-deposited layer), MoO_x, and Al electrode were thermally evaporated under a vapor pressure of 1×10^{-6} torr onto Ta_2O_5 layer. Transient characteristics were measured by using oscilloscope (MDO4000) and the mobility (μ) of the HTLs were obtained by the relationship

$$\mu = \frac{2d_s^2}{At_{tr}^2}\left(1 + \frac{\epsilon_s d_i}{\epsilon_i d_s}\right), \; t_{tr} = \frac{4}{\pi} t_{2j_0}$$

where ϵ_s (ϵ_i) is the relative permittivity of the semiconductor (insulator) and d_s (d_i) is the thickness of the semiconductor (insulator) layer. t_{2j0} is the time to reach the current with off-set bias (U_{off}) to the double of current without off-set bias (j_0).

2.2.5 Morphological analysis of thin films

Surface energy analysis: The contact angles of QDs onto ZnO substrates were measured by the sessile drop method using a contact angle measurement system (Pheonix-300, SEO Corporation) equipped with a video capture apparatus. The surface energy were calculated by the Owen-Wendt method using Young's equation (1), Owen-Wendt equation (2) and equation (3).

$\gamma_{SG} = \gamma_{SL} + \gamma_{LG}\cos\theta$ (1) (Young's equation)

$\gamma_{SL} = \gamma_{SG} + \gamma_{LG} - 2\left(\gamma_{SG}^{d} \cdot \gamma_{LG}^{d}\right)^{\frac{1}{2}} - 2(\gamma_{SG}^{p} \cdot \gamma_{LG}^{p})^{1/2}$ (2) (Owen-Wendt equation)

$\gamma_{SG} = \gamma_{SG}^{d} + \gamma_{SG}^{p}$ (3)

Where γ_{LG} is the surface energy of liquid and gas, γ_{SG} is the surface energy between solid materials and gas, γ_{SG}^{d} is the dispersion component of surface energy and γ_{SG}^{p} is the polar component of surface energy. To determine the surface energy, two measure liquids, for example deionized water (DI) and ethylene glycol (EG), whose surface energy and polar and dispersion components of surface energy are known are used. The polar component of DI is 51 mJ/m^2 with total surface energy 72.8 mJ/m^2 and the polar component of EG is 19 mJ/m^2 with total surface energy 48 mJ/m^2. In order to calculate the surface energy of the analyzed materials (CBP, mCP, and QD films with ligands), the contact angles (θ) with the DI and EG were measured. Then, we obtained γ_{SG} from solving the equation (1), (2), and (3).

Atomic Force Microscopy (AFM): Topography of each film was measured by XE-100 (Park Systems) AFM System. Most of the films were measured in non-contact

mode with NCHR probe tip (320 kHz, 42 N m^{-1}) followed by image processing in XEI v.1.7.1.

2.2.6 Device simulation method

The device simulator SimOLED (v4.2.1) models [62] the electrical behavior of QLED devices by assuming electrical properties of quantum dot as organic materials. The draft-diffusion equation is solved based on the 1-D finite element method (FEM) for holes and electrons and the involved excitons. Followed Poisson equation, continuity equations are numerically solved using FEM.

$$\frac{\partial F}{\partial x} = \frac{q}{\varepsilon \varepsilon_0}(p(x,t) + n(x,t))$$

Poisson equation is expressed as above, while F is the electric field inside the QLEDs, q is the elementary charge, ε is the dielectric permittivity of the organic materials, ε_0 is the dielectric constant, p and n are the charge carrier concentrations for holes and electrons (includes free and trapped charges), respectively. Continuity equation for electron is stated as

$$\frac{\partial n_f(x,t)}{\partial t} = \frac{1}{q}\frac{\partial J_{nf}(x,t)}{\partial x} - R - T,$$

whereas n_f is the charge carrier concentration of free electrons, J_{nf} is the electron current density, R is the recombination rate (between free and trapped carriers), T is the trapping rate for free carriers.

$$\frac{\partial s(x,t)}{\partial t} = \mathrm{c} \cdot \mathrm{R} + D_s \frac{\partial s(x,t)}{\partial x} - \frac{s(x,t)}{\tau_s} - Q$$

Therefore exciton density s is formulated in the above equation whilst c is a factor due to spin statistics (1/4 for singlet, 3/4 for triplet), D_s is the diffusion

constant for excitons, τ_s is the exciton lifetime, and Q is includes quenching terms for excitons (i.e. quenching at contacts, free carriers or excitons).

2.2.7 Other Characterization Methods

UV-Visible Spectroscopy: The transmission and absorption spectra were measured with DU-70 UV/Vis Scanning Spectrophotometer (Beckman Coulter, Inc.) or Agilent 8454 UV-Vis. diode array spectrometer. In case of solution, materials were dissolved in toluene or chlorobenzene. For the film measurement, materials were spin-coated or evaporated thermally in the thickness of ~50 nm on quartz substrate. The reflectance spectra were measured by a Varian Cary 5000 spectrophotometer. The average transmittance (T_{avg}) was calculated by the following equation.

$$T_{\mathrm{avg}} = \frac{\int_{\lambda_1}^{\lambda_2} T(\lambda)\mathrm{d}\lambda}{\lambda_2 - \lambda_1} \tag{2.7}$$

Where $T(\lambda)$ is the transmittance as a function of the wavelength, T_{avg} was usually calculated by integrating $T(\lambda)$ from 400 nm (λ_1) to 800 nm (λ_2).

Ultraviolet Photoelectron Spectroscopy (UPS): The UPS spectra were performed using Kratos AXIS-NOVA, employing He I light source and a hemispherical analyzer. The valence band maximum (VBM) of the nanocrystals was calculated using the following equation.

$$VBM = 21.2\,eV - \left|E_{cutoff} - E_{onset}\right| \tag{2.8}$$

The conduction band minimum (CBM) value was obtained by using the VBM and the excitonic band gaps of QDs, estimated from the PL spectra of QDs.

Film Thickness Measurement: Ellipsometers (L2W15S830 with 632.8-nm He-Ne laser light, Gaertner Scientific Corp. and M2000D, Woollam) and an AFM (XE-100, Park Systems) were used for measuring the thicknesses of films

Transmission electron microscopy (TEM): The TEM images of the QDs were obtained using a Tecnai TF30 ST at 200 KV to analyze their average size and size distribution. The energy dispersive x-ray (EDX) spectra of QDs were acquired through Si-Li detector of Oxford INCA Energy attached on main body of TEM. Low-coverage samples were prepared by placing a drop of a dilute toluene dispersion of QDs on a copper grid (300 mesh) coated with an amorphous carbon film. The composition of QDs was measured with inductively coupled plasma optical emission spectroscopy (Agilent ICP-OES 720).

QDs' general characterization: A photoluminescence quantum yield (PL QY) was acquired in the comparison of their fluorescence intensities with those of primary standard dye solution (coumarin 545, quantum yield = 95 % in ethanol) at the same optical density (below 0.05) at same excitation wavelength (400 nm). For photoluminescence lifetime measurements, the samples were excited at 488nm (pulse width ~ 40 ps) at a repetition rate of 2 MHz. PL dynamics were measured using time-correlated single-photon counting (TCSPC) system that consists of avalanche photodiodes (timing resolution ~ 350 ps) and a multi-channel analyzer (Picoquant Hydraharp).

Chapter 3

Efficient Blue Quantum Dot Light-Emitting Diodes *via* Co-deposited Hole Transport Layer

Since the first QLEDs had been developed, there were considerable efforts to enhance the device performance of QLEDs in terms of bright emission, high luminescence efficiency and low driving voltage for meeting the requirements in the display applications. As fabrication process issues arisen from the solution process of QDs have been settled by adopting cross linkable polymer HTL or thermally evaporable small molecule HTL through inverted structure, studies elucidating relation between device efficiency and electronic properties among each layer of QLEDs have been increased gradually. Researches regarding to device

characteristics of QLEDs imputes the reasons for low efficiency of QLEDs to the non-radiative Auger recombination process that causes excitons in QD to vanish without emitting light. The non-radiative Auger recombination process is promoted by the excess charge carrier in QD originated from charge injection imbalance. Energetic barrier between deep VBE energy level of QDs (~ 7 eV) and relatively shallow HOMO energy level of organic HTL (5-6 eV) hinder efficient hole injection from HTL to QD layer while similar conduction band edge (CBE) energy level of QDs and metal oxide ETL facilitate electron injection from ETL to QD layer. Difference of charge injection rates into QD layer causes excess electron charge carrier within QDs thereby non-radiative Auger recombination process [63, 64]. To solve the charge imbalance problem, various methods have been suggested that cover material development and device structural solution. On the material side, type I core/shell heterostructured QDs whose shell have energetic barrier for electron injection effectively hinders electron injection, which dramatically enhances device efficiency and roll-off characteristics [43]. Increasing shell thickness of QD also elevates the performance of QLEDs [42]. On the device side, insulting interfacial layer that acts as insulating material or dipole layer at the interface of ETL and QD emissive layer works on balancing charge carrier injection [36, 46, 65, 66].

Despite recent advance in device performance of QLEDs, luminescence efficiency of blue-QLEDs is still low compared to red- and green-QLEDs composed of smaller bandgap QDs than blue-QDs. Deeper VBE energy level of blue-QD that consists of larger-bandgap composition likes ZnSe/ZnS [67-69] or $Cd_{1-X}Zn_XS/ZnS$ [33, 44, 70, 71] enlarges hole injection barrier into blue-QDs. Large hole injection barrier creates efficiency drops owing to the non-radiative recombination by charge carrier imbalance and electron overflowing over higher lowest unoccupied

molecular orbital (LUMO) energy level of HTLs. Enhancing hole injection rates into larger-bandgap blue-QD is important to improve the performance of blue-QLEDs.

In Chapter 3, we conduct systematic studies to investigate correlation between electrical characteristics of HTL and device characteristics of blue-QLEDs using commercially available HTLs. Then we proposed the co-deposition of CBP and mCP for the HTL of blue-QLEDs. Suggested device exhibits improved hole injection rates and device efficiency rather than reference device through higher LUMO energy level and hole density of CBP:mCP co-deposited layer.

3.1 Larger-bandgap QDs based LEDs made of a series of HTLs with different HOMO Energy Levels.

We have synthesized $Cd_{1-X}Zn_XS/ZnS$ core/shell heterostructured QDs for emissive material of blue-QLEDs. Synthesized QD is composed of core radius = 2.0 nm and shell thickness = 2.3 nm and stabilized with oleic acids that allow QDs dispersed in toluene solvent and preserve aggregation of QDs. Transmission electron microscopy (TEM) image of QDs shows the uniform distribution of synthesized QDs and photoluminescence (PL) spectra of $Cd_{1-X}Zn_XS/ZnS$ core/shell heterostructured QDs is centered at 450 nm. Ultraviolet photoelectron spectroscopy (UPS) measurement shows large energy barrier between blue-QDs and organic HTLs. Hole injection barrier arisen from difference between VBE energy level of QD and HOMO energy level of HTL leads hindrance of efficient hole injection from HTL into QDs [72, 73] while similar CBE energy level of QDs and ZnO ETL allows facilitated electron injection from ETL into QDs. Injected charge carrier imbalance within QD emissive layer cause non-radiative Auger recombination process. To figure out relation between HOMO energy level of HTL and the device characteristics of blue-QLEDs, we screen the commercially available HTLs spreading HOMO energy level range from 5.4 eV to 6.0 eV . N,N'-Di(1-naphthyl)-N,N'-diphenyl-(1,1'-biphenyl)-4,4'-diamine (NPB) [74, 75], 4,4'-Cyclohexylidenebis[N,N-bis(4-methylphenyl)benzenamine] (TAPC) [76, 77], Tris(4-carbazoyl-9-ylphenyl)amine (TCTA) [78, 79], 4,4´-Bis(N-carbazolyl)-1,1´-biphenyl (CBP) [80] or 1,3-Bis(N-carbazolyl)benzene (mCP) [81, 82] are treated as HTL of QLED.

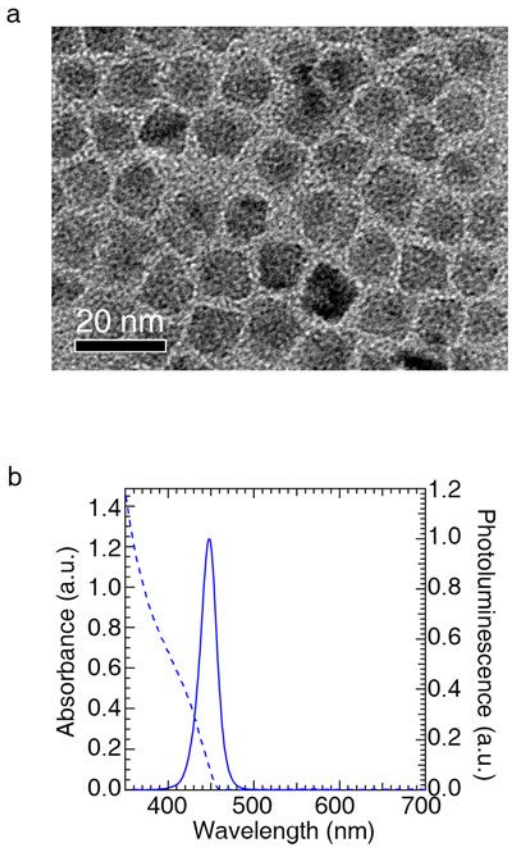

Figure 3.1 (a) Transmission electron microscopy (TEM) images and (b) absorbance and photoluminescence spectra of $Cd_{1-X}Zn_XS$(r = 2 nm)/ZnS(h = 2.3 nm) blue QDs.

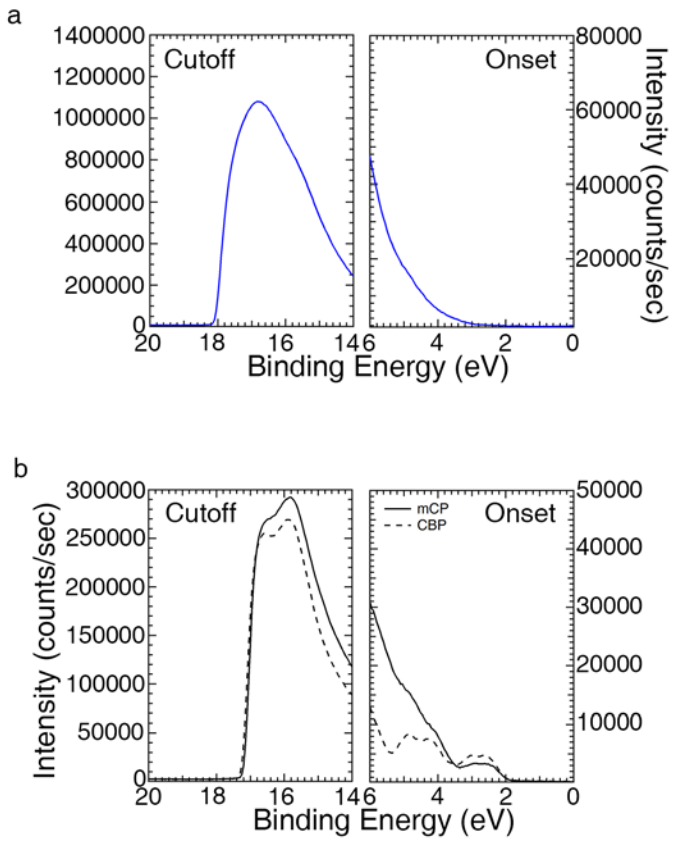

Figure 3.2 Ultraviolet photoelectron spectroscopy (UPS) spectra of (a) blue QDs, (b) mCP (solid line) and CBP (broken line) on ITO substrates.

Table 3.1 HOMO energy level, LUMO energy level characteristics of hole transport layers.

	HOMO (eV)	**LUMO (eV)**	**reference**
mCP	6.0	2.4-2.5	This work, 81, 82
CBP	6.0	2.9	This work, 79, 80
TCTA	5.7	2.4	74, 76, 77, 78
TAPC	5.5	2.0	74, 75
NPB	5.4	2.3	78, 79

3.2 Characteristics of electroluminescence devices with various HOMO energy level.

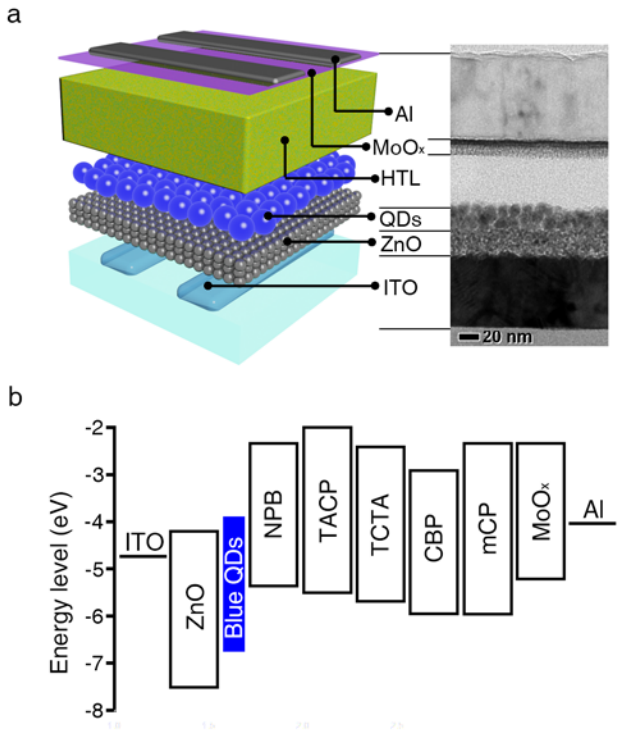

Figure 3.3 (a) Schematic illustration (left) and cross-sectional transmission electron microscopy (TEM) image (right) of blue QLED. (b) Energy level diagram of blue QLEDs employing NPB, TAPC, TCTA, CBP or mCP as HTL.

Figure 3.3a shows the inverted structure of QLEDs in a configuration of ITO//ZnO//QDs//HTL//MoOx//Al. NPB, TAPC, TCTA, CBP and mCP are chosen to their various HOMO energy level. Energy level of each layer is illustrated in Figure 3.3b. The device characteristics of blue-QLEDs using NPB, TAPC, TCTA, CBP or mCP is displayed in Figure3.4. The Maximum E.Q.E.s of each device are 0.2 %, 1.1 %, 1.4 %, 1.3 % and 0.01 % for device with NPB, TAPC, TCTA, CBP

and mCP, respectively. The E.Q.E. of device is increased as the HOMO energy level of HTL ascends. The turn-on voltage (operation voltage of device at the brightness of 1 cdm^{-2}) and driving voltage (operation voltage of device at the brightness of 100 cdm^{-2}) of each device is (4.1 V, 6.5 V), (4.5 V, 5.9 V), (3.6 V, 5.0 V), (3.5 V, 4.8 V) and (4.0 V, -) for device with NPB, TAPC, TCTA, CBP and mCP, respectively. The turn-on voltage and driving voltage of device is reduced as the HOMO energy level of HTL is increased. This result means that lowering energetic barrier between VBE energy level of larger-bandgap blue-QD and HOMO energy level of HTL enhances the hole injection rates thereby the efficacy of device.

Almost device characteristics of QLEDs agree with out anticipation but that of QLEDs using mCP does not follow our expectation. QLEDs with mCP shows almost 0 % E.Q.E. Turn-on voltage of QLEDs with mCP is 4.0 V higher than QLEDs with CBP and driving voltage of QLEDs with mCP could not be measured because the max brightness does not reach to 100 cdm^{-2}. The device performance of QLEDs using mCP does not agree with the tendency because HOMO energy level of mCP is same as that of CBP. We conduct the morphological analysis to figure out the reason of extremely low efficiency of device with mCP.

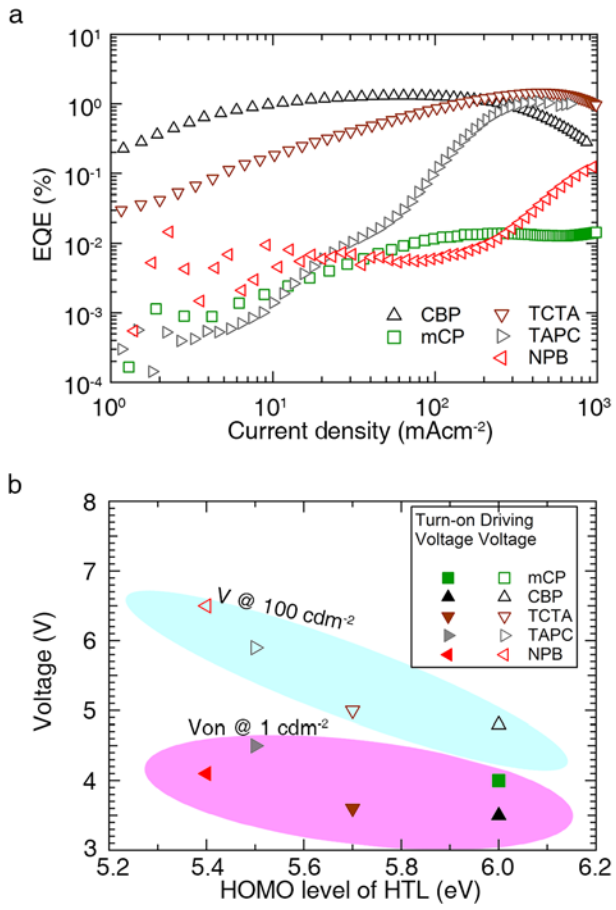

Figure 3.4 (a) External quantum efficiency (E.Q.E.) characteristics of blue QLEDs with different HTLs (leftward triangle, rightward triangle, downward triangle, square or triangle symbol for NPB, TAPC, TCTA, mCP or CBP). (b) Turn on voltage corresponds to the brightness of 1 cdm^{-2} (closed symbol) and driving voltage corresponds to the brightness of 100 cdm^{-2} (open symbol) of blue QLEDs with various HTLs.

3.3 Influence of surface energy differences between QDs and HTLs on the morphological profiles of HTL films

CBP and mCP have similar hole injection barrier into blue-QDs but blue-QLEDs using mCP shows severely low device efficiency of 0.01 % E.Q.E. and maximum brightness of 45 cdm^{-2}. To investigate the difference between blue-QLEDs with CBP or mCP, morphological analysis is conducted. The atomic force microscopy (AFM) measurements bear out the reason of low luminescence efficiency of device with mCP. The morphological inhomogeneity of mCP largely affects the device characteristics of blue-QLEDs. We analyze the surface roughness (root mean square, RMS) of each layer step-by-step during fabrication of blue-QLEDs through AFM measurements. The result of AFM analysis is shown in Figure 3.5. The RMS value of bare ITO surface is 0.73 nm. The RMS value increases to 0.98 nm after ZnO layer spin-coated. The RMS value after spin-coating blue-QDs is 0.86 nm. After thermal evaporation of mCP, the RMS value changes to 33.20 nm while evaporation of CBP layer changes the RMS value to 2.89 nm. The RMS value of mCP in device is 11 times larger than that of CBP in device. Moreover, although we deposited 60 nm of the mCP layer by controlling using quartz crystal microbalance (QCM), peak-to-valley value of mCP layer is 140.50 nm higher than evaporated thickness owing to the aggregation of mCP layer onto QD layer during evaporation. Electrons leak into counter electrode *via* direct contact between QD layer and MoOx/Al electrode due to the island growth of mCP layer, which causes the significant efficiency loss in the device. The surface energy difference between evaporating material and underlying layer affects the growth behavior of HTL during thermal evaporation [83, 84]. The surface energy of each layer is calculated by Owens & Wendt model combined with the contact angle. Huge difference of

mCP (γ = 24.85) and QDs (γ = 32.21) causes morphological inhomogeneity, whereas similar surface energy level of CBP (γ = 32.12) makes an uniform layer on top of QD layer. We thermally evaporate CBP and mCP simultaneously to avoid the morphological inhomogeneity. CBP:mCP co-deposited layer shows the similar surface energy value (γ = 33.12) with the QD layer. As a result, we could obtain smaller RMS value of CBP:mCP co-deposited layer (1.16 nm) after evaporating onto QD layer than that of CBP and subsequent layer deposited uniformly.

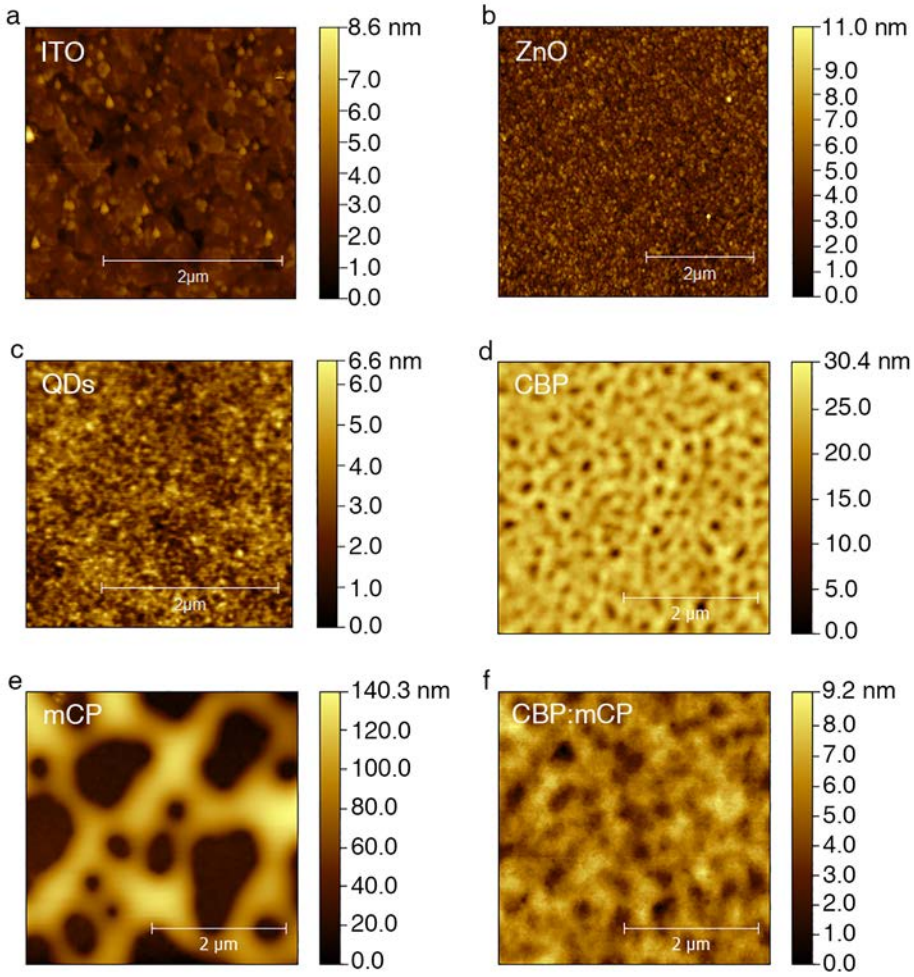

Figure 3.5 AFM images of (a) ITO, (b) ZnO, (c) blue-QDs and (d-f) different HTLs evaporated on top of QDs. (d) CBP, (e) mCP and (f) CBP:mCP co-deposited layer are used as HTLs.

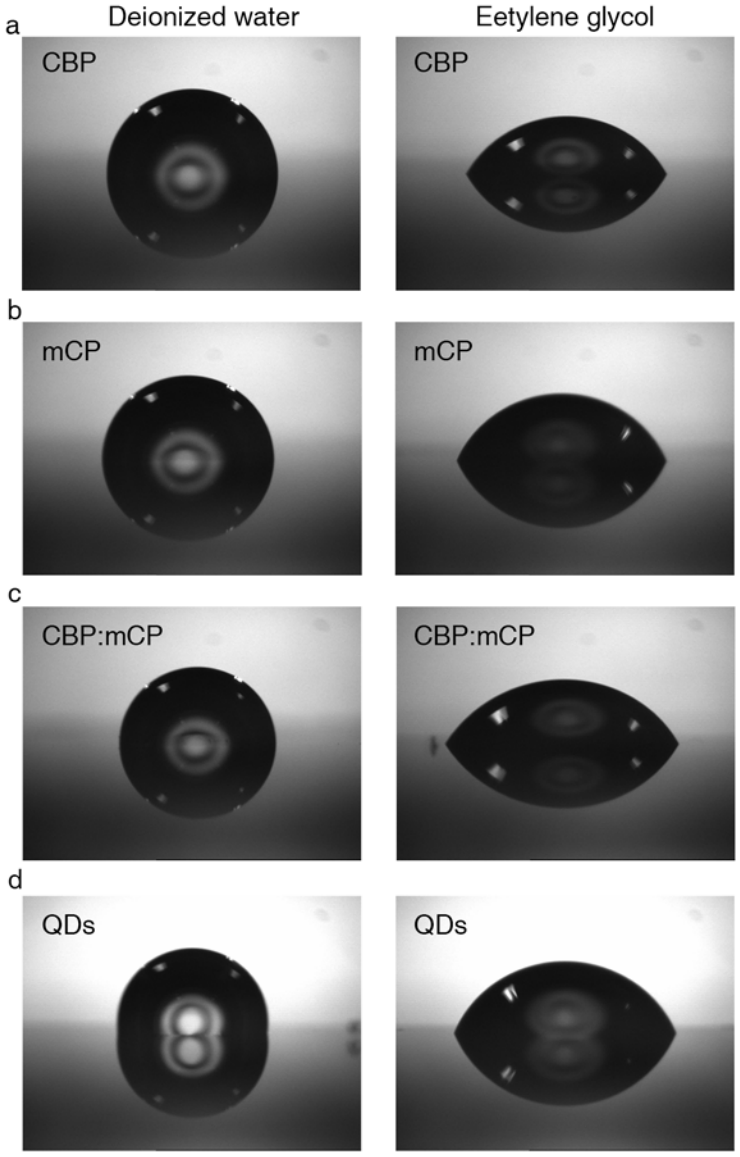

Figure 3.6 Photograph of deionized water (left) and ethylene glycol (right) droplets on top of (a) CBP (b) mCP (c) CBP:mCP and (d) QDs for measuring the contact angles between droplet and thin films.

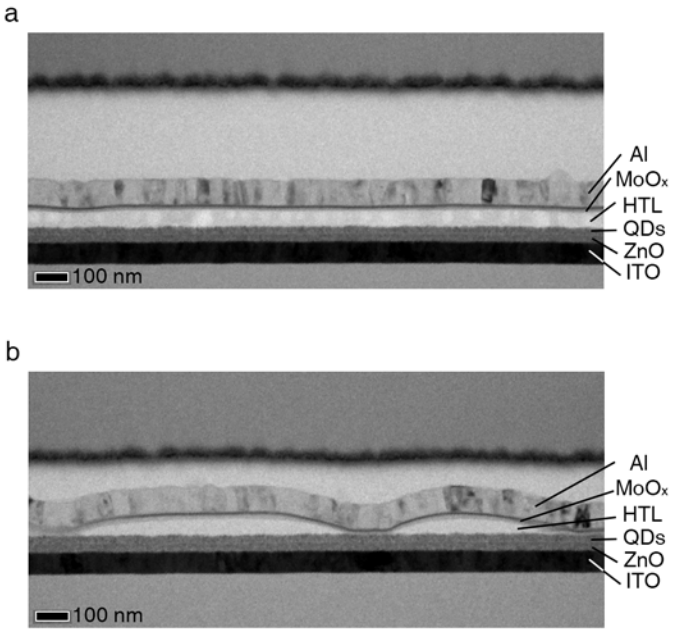

Figure 3.7 (a) Cross-sectional TEM images of QLEDs with (a) CBP:mCP co-deposited layer and (b) mCP.

Table 3.2 Surface energy for different HTLs and QDs calculated from contact angle.

	CBP	**mCP**	**CBP:mCP**	**QDs**
γ (mJm^{-2})	32.119	24.852	33.120	32.206
γ^d (mJm^{-2})	29.491	18.709	30.263	31.495
γ^p (mJm^{-2})	2.628	6.143	2.857	0.7111

3.4 Characteristics of electroluminescence devices made of carbazole derivatives co-deposition layer.

Fabricated inverted structure blue-QLEDs with CBP:mCP co-deposited layer shows uniform morphologies. After evaluating the device characteristics of blue-QLEDs with the line-up of HTLs (Figure 3.3), we narrow down candidates for HTLs of blue-QLEDs to CBP and CBP:mCP co-deposited layer. Organic HTLs with HOMO energy levels less than 6.0 eV are excluded, because such HTLs do not ensure sufficient hole injection into blue-QDs whose VBE energy level locates at 6.7 eV (Figure 3.2), as reflected by the increase in the turn-on voltage and the decrease in the device efficiency of blue-QLEDs (Figure 3.4). To optimize the volume ratio of CBP and mCP in the co-deposited layer, we fabricated the blue-QLEDs. CBP:mCP co-deposition layer was used for the HTL in the devices. We screened evaporated volume ratio of CBP from 25 vol% to 75vol% in the CBP:mCP co-deposited layer. Devices had configuration of ITO/ZnO/blue-QD/co-deposited HTL/MoOx/Al.

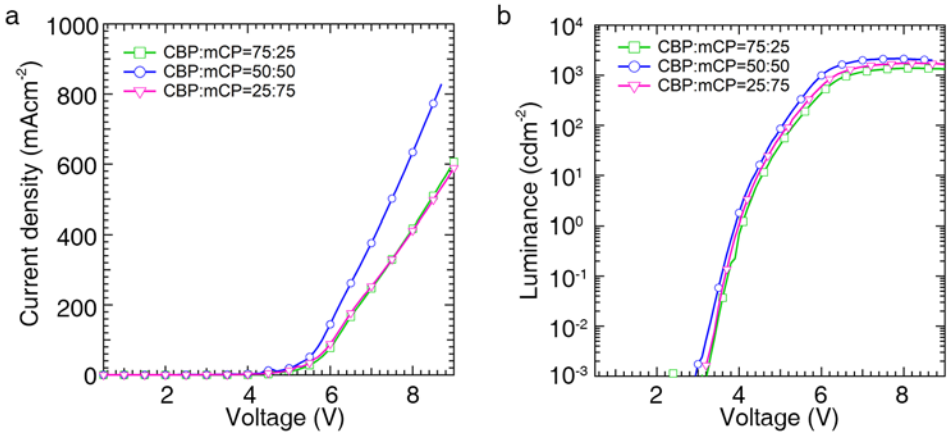

Figure 3.8 (a) Current density (*J*)-voltage (*V*) characteristics, (b) luminance (*L*)-*V* characteristics of blue QLEDs with CBP:mCP co-deposited layer. The volume ratios of CBP from 25 vol% to 75vol% in the CBP:mCP co-deposited layer are screened.

Figure 3.8 shows the current density (*J*) – voltage (*V*) and luminance (*L*) - *V* characteristics of the devices fabricated with the different CBP and mCP deposition ratios. It is clearly observed that the current density and luminance of the devices show highest value in the device with 1:1 volume ratio of CBP:mCP co-deposited layer. Current densities at operation voltage 6 V are 88.3 $mAcm^{-2}$, 144.2 $mAcm^{-2}$ and 77.3 $mAcm^{-2}$ for the devices with 25 vol%, 50 vol% and 75vol% of CBP, respectively. Each device exhibits luminance of 602 cdm^{-2}, 993 cdm^{-2} and 441 cdm^{-2} at the same operational voltage for the devices with with 25 vol%, 50 vol% and 75vol% of CBP. This results indicates that the 1 to 1 volume ratio of CBP and mCP co-deposited layer can transport hole carrier from MoOx/Al electrode to interface of blue-QDs and HTL efficiently compared to the different composition of CBP and mCP co-deposited layer.

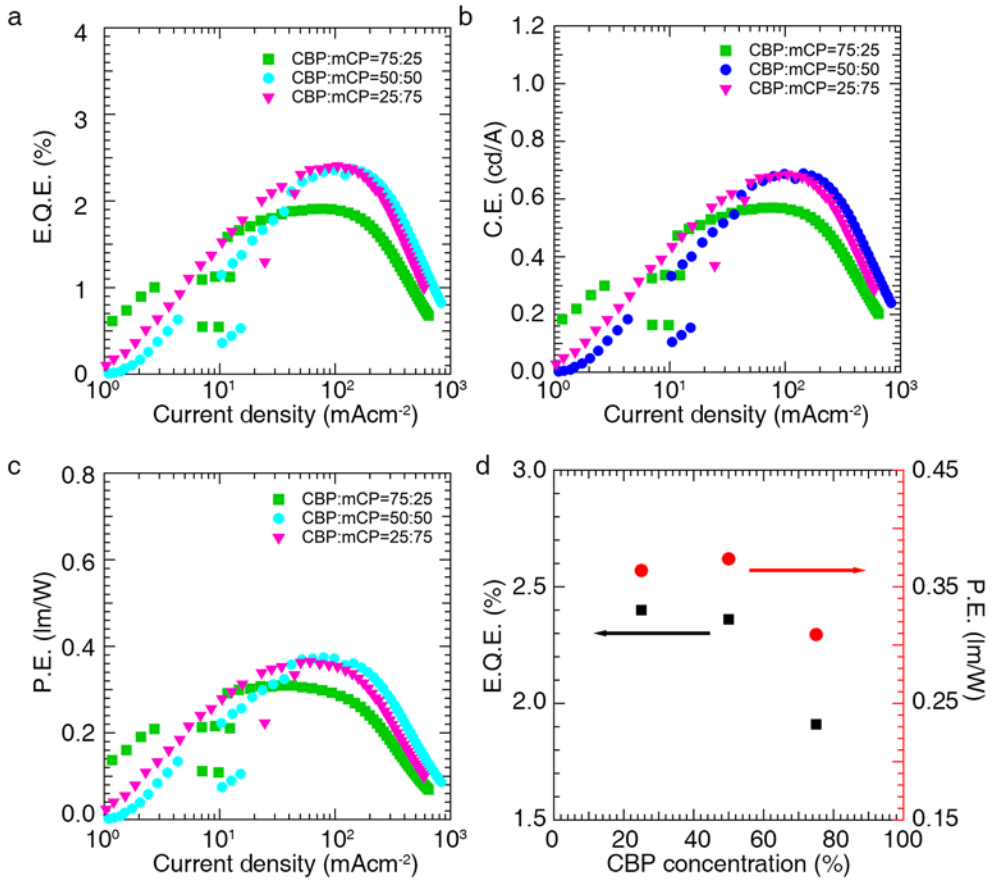

Figure 3.9 (a) E.Q.E., (b) current efficiency (C.E.) and (c) power efficiency (P.E.) *versus J* of blue QLEDs with CBP or CBP:mCP co-deposited layer with CBP volume ratio from 25 vol% to 75vol%. (d) Maximum E.Q.E. and P.E. of devices with CBP volume ratio ranging from 25 vol% to 75vol%.

The device performance in terms of E.Q.E., current efficiency (C.E.) and power efficiency (P.E.) *versus J* are shows in Figure 3.9. The efficiencies of device with 25 vol% and 50 vol% of CBP are quite similar. The E.Q.E.s of devices with 25 vol% and 50 vol% of CBP are 2.40 % and 2.36 % at maximum points, corresponding to

0.686 cd/A and 0.688 cd/A in C.E. and 0.364 lm/W and 0.374 lm/W in P.E., respectively. The device with 75 vol% of CBP shows lower efficiency of 1.91 % in E.Q.E., 0.570 cd/A in C.E. and 0.309 lm/W in P.E. This results indicate that the small amount of mCP in CBP:mCP co-deposited layer could not affect the device characteristics. The E.Q.E. of device with 50 vol% CBP is slightly low compared to that of device with 25 vol% CBP but the C.E. and P.E. of devices with 50 vol% CBP come from behind owing to the higher current density in the device with 1:1 CBP and mCP volume ratio. Lower operation voltage of devices also affects the operational stability of blue-QLEDs. The decrease of luminance in the device is illustrated in Figure 3.10 where the initial luminance is 500 nit. Lower operational voltage of blue-QLED with 1:1 CBP and mCP co-deposited layer allows the lower driving power at the same initial luminance (0.436 Wcm^{-2}, 0.420 Wcm^{-2} and 0.532 Wcm^{-2} for 25 vol%, 50 vol% and 74 vol% of CBP, respectively). The device using 1:1 CBP and mCP co-deposited layer exhibits longer lifetime (i.e. the luminance half-life time (T50) = 0.31 hr) compared to the device using other depositing volume ratios (T50 = 0.18 hr) due to the low operation power and high device efficiency.

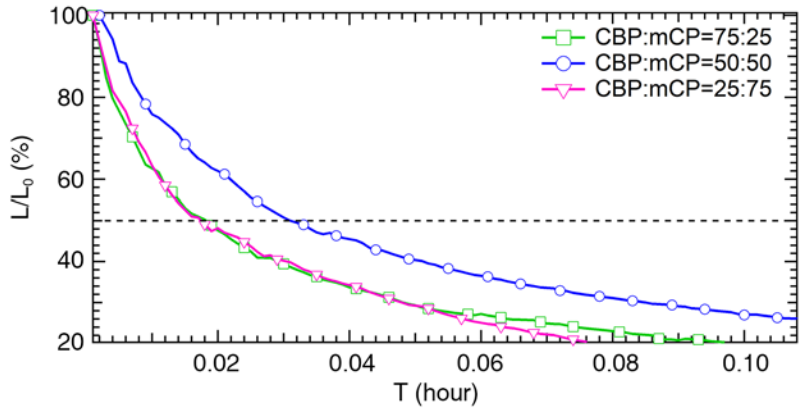

Figure 3.10 Operational stability test results of blue QLEDs with CBP:mCP (1:1) co-deposited layer. Initial luminance (L_0) of QLEDs is 500 cdm^{-2}.

After optimizing the device characteristics of blue-QLEDs with CBP and mCP depositing volume ratio, we compare the device characteristics of blue-QLEDs using CBP and 1:1 CBP and mCP co-deposited layer, whose HOMO energy levels (6.0 eV, Figure 3.2) position close to the VBE energy levels of blue-QDs (6.7 eV, Figure 3.2). Figure 3.11 contrasts the device characteristics of blue QLEDs using CBP versus CBP:mCP co-deposited layer. Blue QLEDs implementing CBP:mCP co-deposited layer exhibit the reduction in the driving voltage, and the enhancement in the current density and the brightness (Figure 3.11a, b). Specifically, the driving voltages and the current densities at the peak E.Q.E. descend from (5.6 V, 63.827 $mAcm^{-2}$) to (5.0 V, 59.694 $mAcm^{-2}$). Furthermore, as a result of the dockage in the operational voltage, the power consumption also reduced in QLEDs utilizing CBP:mCP co-deposited layer. Specifically, blue-QLEDs using CBP:mCP co-deposited layer show 0.7 V of reduction in the driving voltage for emitting the luminance of 100 cdm^{-2}. These results confirm the role of CBP:mCP co-deposited HTL in the enhancement in the hole injection rate into QDs emissive layer and the improvement of the optoelectronic performance. Blue-QLED with CBP:mCP co-deposited layer displays increase in the current density and the E.Q.E. by a factor of 2 than that with blue-QLED with CBP (Figure 3.11a, c). Moreover, the employment of CBP:mCP co-deposited layer suppresses surface-related broad-band EL emission in the spectra (Figure 3.11d). These results represent that the use of CBP:mCP co-deposited layer enhances the hole injection rate into the emissive core of the larger bandgap blue QDs and the luminescence efficiency of larger bandgap blue QDs.

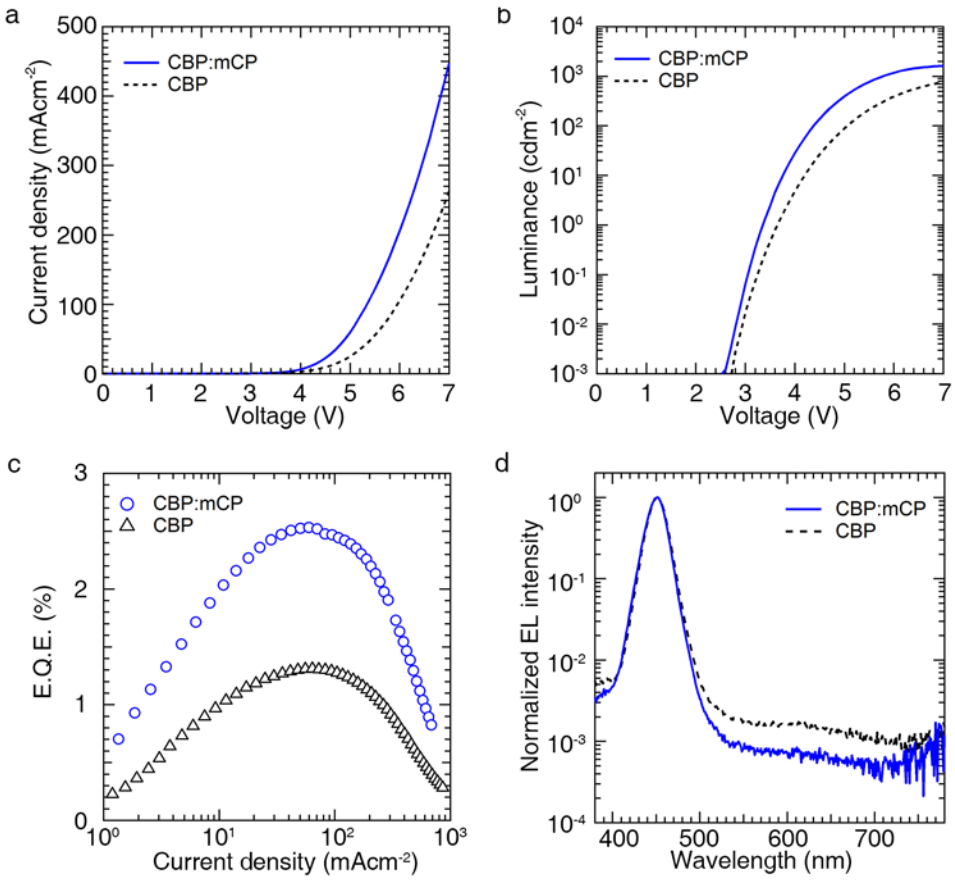

Figure 3.11 (a) *J* - *V* characteristics, (b) *L* - *V* characteristics and (c) E.Q.E. *versus J* of blue QLEDs with CBP or CBP:mCP (1:1) co-deposited layer. (d) Normalized electroluminescence (EL) spectra of QLEDs with CBP or CBP:mCP (1:1) co-deposited layer at operating current densities of 10 $mAcm^{-2}$.

Table 3.3 Summary of device characters for the blue QLEDs employing CBP:mCP co-deposited layer or CBP sole layer as HTL.a

HTL	λ (nm)	V_{on} (V)	V_D (V)	Max E.Q.E. (%)	Max C.E. (cdA^{-1})	Max P.E. (lmW^{-1})	Max L (cdm^{-2})
CBP:mCP	451	3.3	4.4	2.53	0.66	0.43	1613
CBP	451	3.5	4.8	1.31	0.38	0.22	880

[a)] Abbreviations: turn-on voltage (V_{ON}), driving voltage (V_D), luminance (L), current efficiency (*C.E.*), power efficiency (*P.E.*).

3.5 Electrical characteristics of co-deposited hole transport layer

The energetic barrier for hole charge injection into QDs from HTLs is defined by the energy level difference between HOMO energy level of hole transporting material and VBE energy level of the QDs and the distance between the QD layer and the HTL. Since the HOMO energy level is identical for both CBP, mCP and thereby CBP:mCP co-deposited layer, two-fold increase of current density and E.Q.E. in QLEDs employing CBP:mCP co-deposited layer implies the enhancement of hole injection rate from HTL into QDs. The hole injection rate is deduced to depend on the hole density (p) and local electric field on the side of HTLs nearby blue QDs. We have calculated the hole density of HTLs from the following relationship with mobility (μ) and the conductivity (σ).

$$\sigma = p \times e \times \mu \quad (\text{where } e = 1.602 \times 10{-}19 \text{ C})$$

The mobility of HTLs is measured by transient signal of dark injection measurement using a hole only devices (HODs, ITO//PEDOT:PSS//HTL//MoOx//Al) structure and the conductivity of HTLs is obtained from the *J-V* characteristics of HODs with CBP, mCP or CBP:mCP co-deposited layer. [85, 86]. Then charge extraction by linearly increasing voltage (CELIV) technique in a metal-insulator-semiconductor (MIS) diode structure (MIS-CELIV) is utilized to cross check the mobility of HTLs [87] (Figure 3.12-14, Table 3.4).

Given that CBP:mCP co-deposited layer holds higher hole density (pCBP:mCP = 6.74 × 1011 cm^{-3}) than CBP (pCBP = 1.95 × 1011 cm^{-3}), blue QLED using CBP:mCP co-deposited layer is expected to exhibit enhanced performance than the case of one using CBP. To better understand the origin of the increase in hole density at CBP:mCP co-deposited layer, we have measured the hole injection

efficiency from anode into HTLs. For that purpose, we have fabricated HODs implementing CBP:mCP co-doposited layer and CBP. We have estimated the hole injection efficiency by comparing *J-V* characteristics of devices with the theoretical space charge limited current density (J_{SCL}).

$$\eta_{\text{injection}} = \frac{J_{exp}}{J_{SCL}}$$

$$J_{SCL} = \frac{8}{9}\epsilon\mu\frac{V^2}{d^3}$$

where J_{exp} is experimental steady-state current density.

The hole injection efficiency from anode to CBP:mCP co-deposited layer is almost 3 times higher than the case with CBP only (Figure 3.15). This result is consistent with the impedance spectroscopic analysis (Figure 3.16) that displays CBP:mCP hold 3 times lower contact resistance than the case with CBP only. Impedance spectroscopic analysis reveals that CBP:mCP co-deposited layer retains less contact resistance with MoOx/Al anode and bulk resistance compared to these with CBP (Figure 3.16, Table 3.5). The decline in the electrical resistivity enlarges the hole density in HTL, amplifies the hole injection rates from HTL into QDs and consequently improves the performance of blue QLEDs, as signified by the enhancement in the current density and the improvement of the device efficiency.

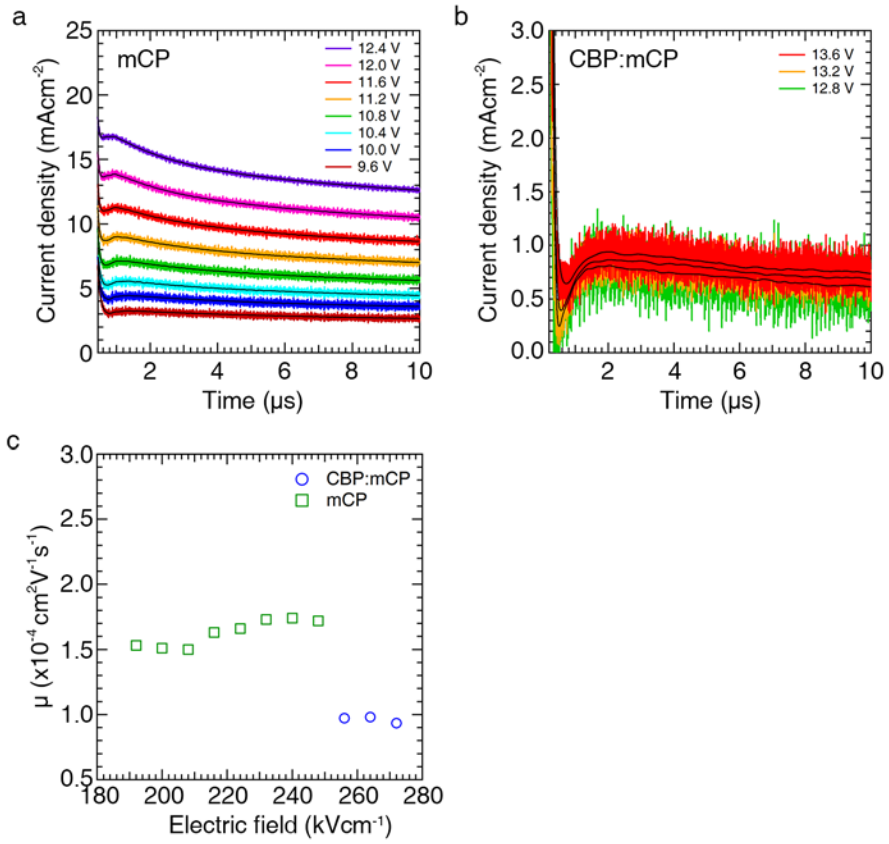

Figure 3.12 Dark injection transient signals for hole-only device with HTLs. The structure of all device is ITO//PEDOT:PSS//HTL//MoOX//Al. Colored line is transient signals of the device and black lines are smoothed signals. (a) Transient signal of device with mCP. (b) Transient signal of device with CBP:mCP co-deposited layer. (c) The mobility of CBP:mCP co-deposited layer and mCP extracted from dark injection transient signals.

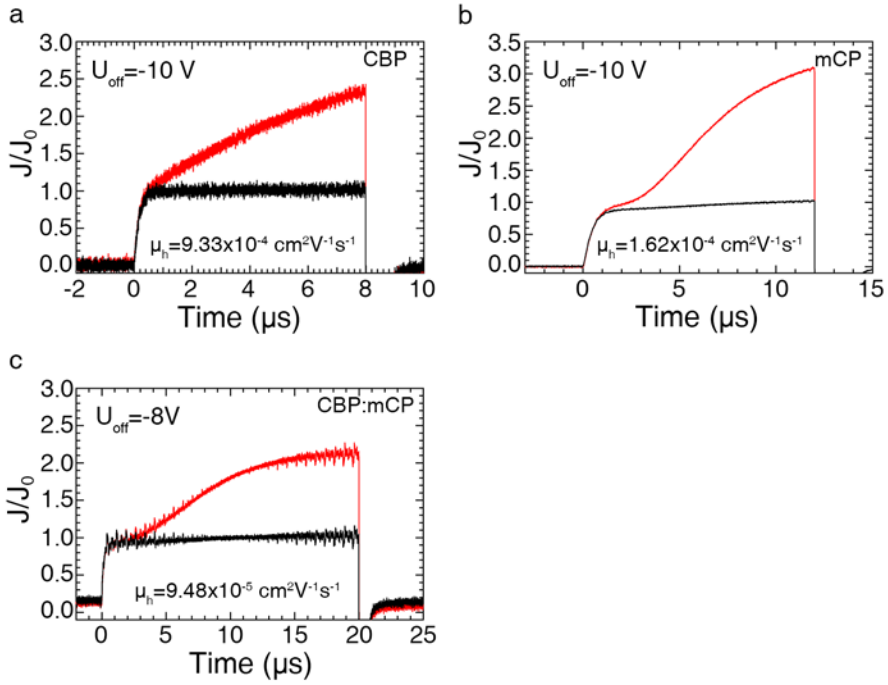

Figure 3.13 Transient signals for the charge extraction by linearly increasing voltage (CELIV) technique in a metal-insulator-semiconductor (MIS) diode structure (MIS-CELIV) with HTLs (CBP, mCP or CBP:mCP co-deposited layer). The structure of all devices is ITO/Ta_2O_5/HTL/MoO_x/Al. Black lines are transient signals of the devices without offset voltage and red lines are signals with offset voltage (U_{off}). MIS-CELIV transient signals of devices with (a) CBP, (b) mCP and (c) CBP:mCP co-deposited layer.

Table 3.4 Mobility characteristics of charge transport layers.

	Mobility ($cm^2V^{-1}s^{-1}$)	**reference**
CBP:mCP	9.73×10^{-5}	This work
mCP	1.63×10^{-4}	This work
CBP	1.0×10^{-3}	This work
ZnO	1.34×10^{-3}	33

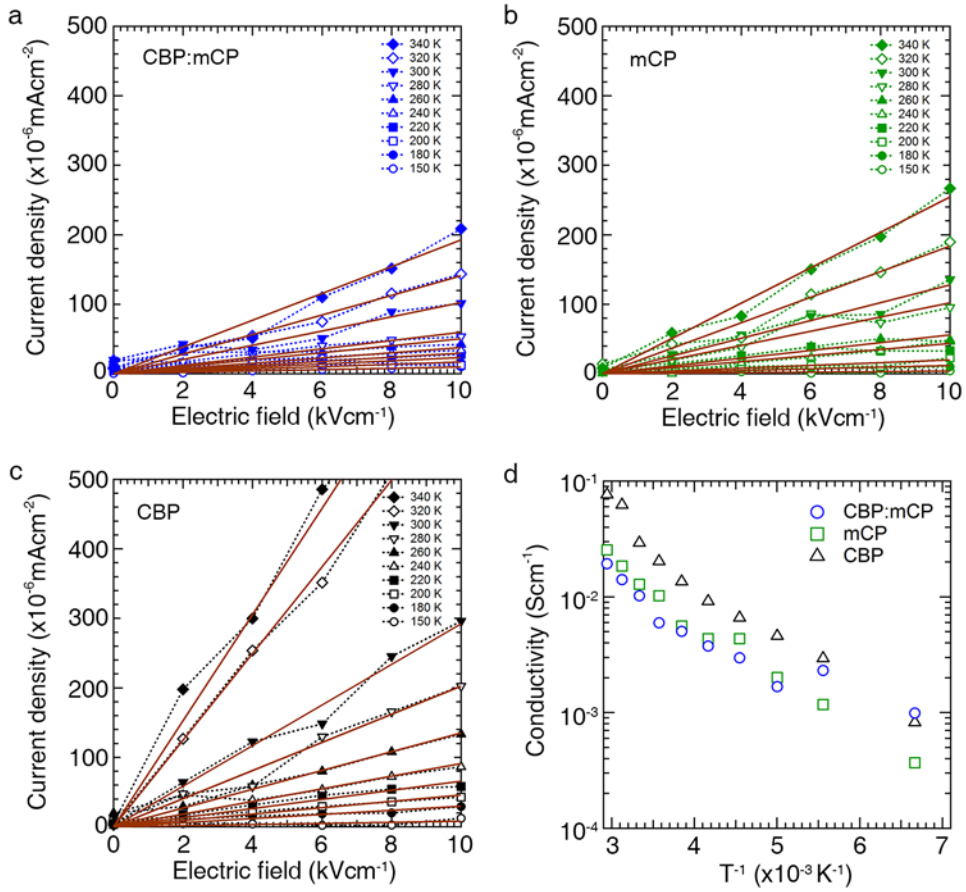

Figure 3.14 Current density-electric filed characteristics for hole only devices with (a) CBP, (b) mCP or (c) CBP:mCP co-deposited layer under 10 kV/cm. Experimental data (colored dotted lines with marker) are fitted line function (brown line). (d) Temperature dependence of the conductivity of devices.

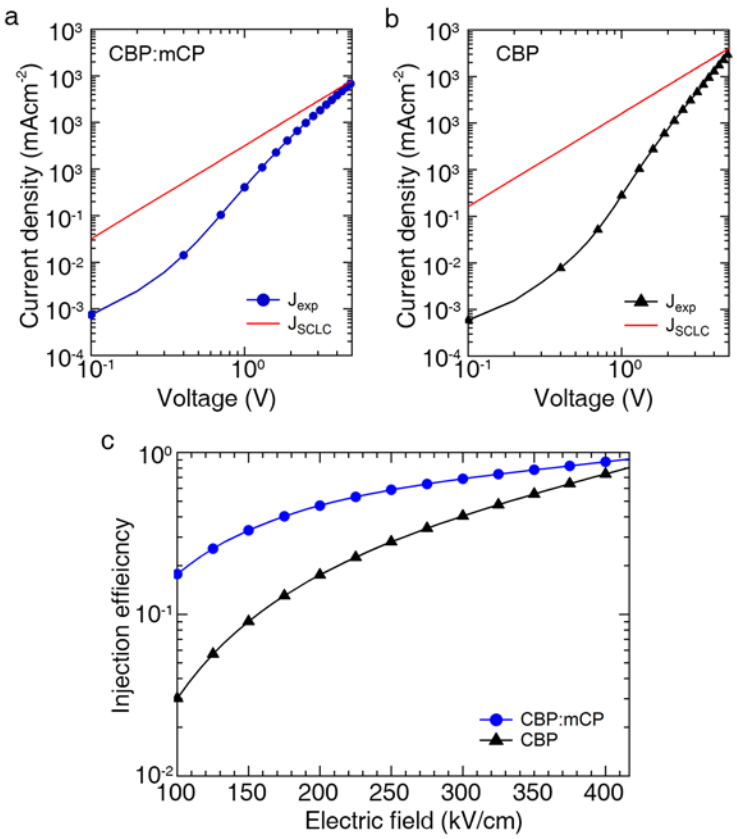

Figure 3.15 *J-V* characteristics for hole only devices with (a) CBP:mCP co-deposited layer versus (b) CBP. Theoretical space-charge limited current density (J_{SCL}) (red line) are overlaid for comparison. (c) Calculated injection efficiency of hole only devices employing CBP:mCP co-deposited layer and CBP sole layer.

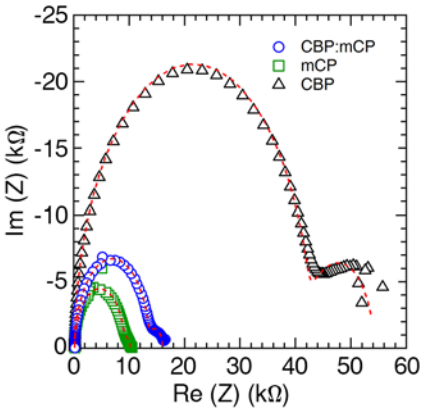

Figure 3.16 The Cole-Cole plots for hole-only devices with various HTLs. Devices with CBP, mCP or CBP:mCP co-deposited layer are fitted by a two-RC model and dashed lines are the fitting line.

Table 3.5 Resistance and capacitance parameters of hole only devices with CBP, mCP and CBP:mCP co-deposited layer extracted using a two-RC model.

	CBP	**mCP**	**CBP:mCP**
$R_{contact}$ (Ω)	2.05×10^{2}	1.98×10^{2}	2.11×10^{2}
$R_{Interface}$ (Ω)	4.23×10^{4}	8.89×10^{3}	1.34×10^{4}
$C_{Interface}$ (F)	9.88×10^{-11}	1.42×10^{-10}	1.26×10^{-10}
R_{Bulk} (Ω)	1.16×10^{4}	1.08×10^{3}	2.44×10^{3}
C_{Bulk} (F)	2.62×10^{-8}	3.88×10^{-8}	4.34×10^{-8}

A side to side with enlarged hole density, higher LUMO energy level of CBP:mCP co-deposited layer also affect the lower driving voltage of blue QLEDs compared to QLEDs using CBP sole layer. Since the height of charge injection barrier between larger-bandgap QDs and HTL that have HOMO energy level 6.0 eV is higher than that between blue QDs and ZnO ETL, electrons are accumulated after injected into QDs. Accumulated electrons are deteriorated by subsequent draft injection through HTL under the forward bias or non-radiative recombination by negative trion or multi-exciton formation. Diminution of accumulated electrons in QD layer is not dominant by Auger recombination at the low current density regime because the low chance of locating electron and exciton in single QD. Major of injected electrons disappear by transporting to CBP and counter electrode or recombine at the HTL that appears in the EL spectra in the high energy region around 400 nm or in the broad-band, surface-related EL emission (Figure 3d). Higher LUMO energy level of CBP:mCP co-deposited layer obstructs the leakage current flow of electron to HTL and confine electron within QDs layer (Figure 6b). Amplified population of electron in QDs layer boosts local electric field from QDs to Al anode, in the aftermath, local electric field from ITO cathode to QDs is enfeebled (Figure 3.17). The enhanced electric field from QDs to Al anode increases hole current density of QLEDs and the relieved local electric field from ITO cathode to QDs decreases electron current density of blue QLEDs (Figure 3.18) [88, 89]. As a result, The use of CBP:mCP co-deposited layer in larger-bandgap blue QLEDs accomplish the control over electron and hole injection from the electrode to the QD emissive layer then improve the electron-hole balance within QDs.

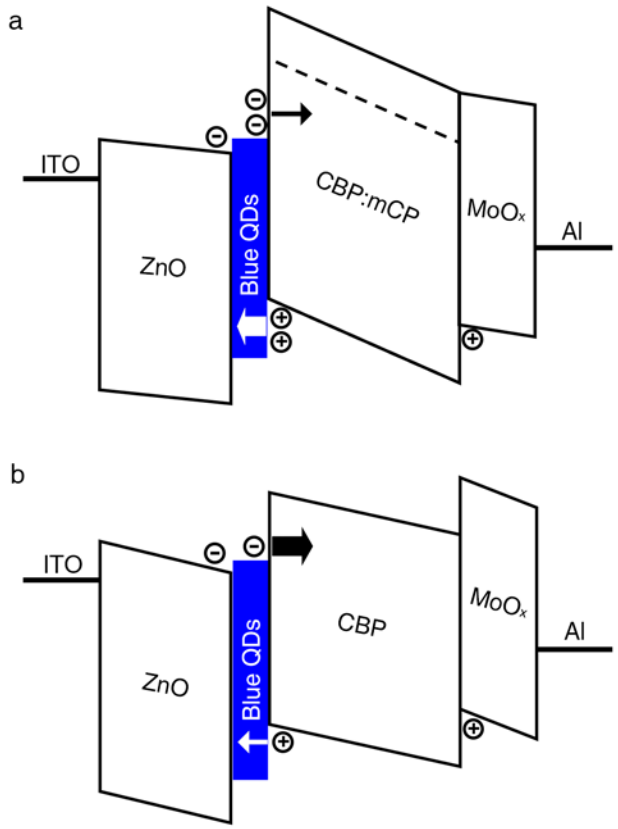

Figure 3.17 Energy band diagrams of blue-QLEDs employing (a) CBP:mCP (1:1) co-deposited layer and (b) CBP sole layer under operation condition.

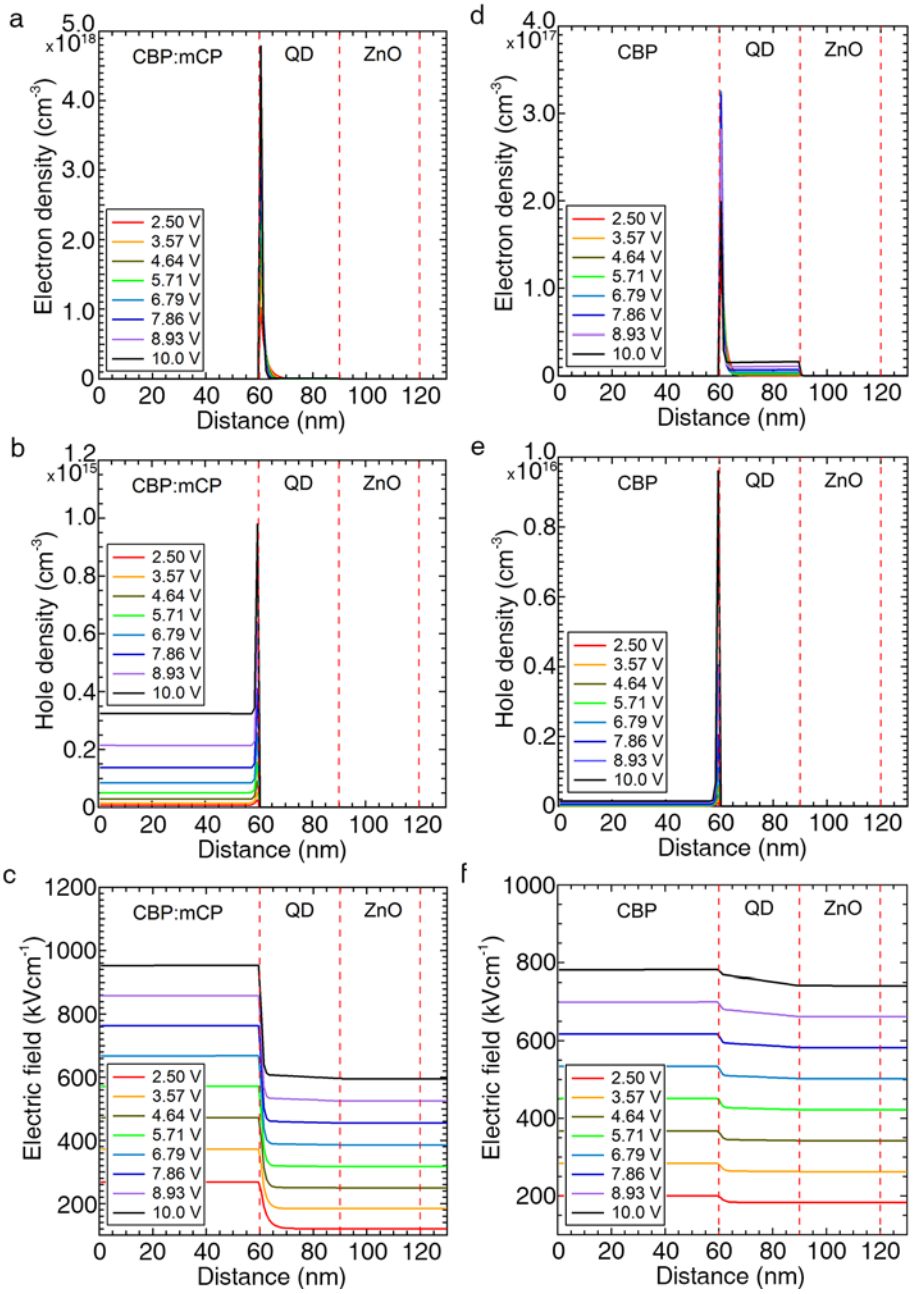

Figure 3.18 Simulation results QLEDs using CBP:mCP co-deposited layer and CBP sole layer. (a,d) Electron density, (b,e) hole density and (c,f) electric field of devices with (a,b,c) CBP:mCP co-deposited layer or (d,e,f) CBP are simulated on operation condition from 2.5 V to 10.0 V.

3.6 Characteristics of electroluminescence devices made of carbazole derivatives bilayer.

We fabricate and characterize the blue-QLED that employs bilayer of CBP and mCP as the HTL of device with configuration of ITO/ZnO/blue-QD/CBP/mCP/ MoOx/Al then compare with the blue-QLED employing CBP:mCP co-deposited layer. The performance of devices are shown in figure 3.19. This configuration of device has the interface blue-QD/CBP and mCP/anode. Comparing the blue-QLED with co-deposited layer and bilayer of CBP and mCP let us know the role of high LUMO energy of HTL in the device. The operation voltage of device with CBP and mCP bilayer relatively increase rather than that with CBP:mCP co-deposited layer. For the device with CBP and mCP bilayer, the driving voltage at 100 $mAcm^{-2}$ is 6.35 V. For the device with CBP:mCP co-deposited layer, the driving voltage at 100$mAcm^{-2}$ is 6.26 V. The efficiency of devices are quite different. The highest values of E.Q.E. are 2.24 % and 2.58 % for blue-QLEDs with bilayer and co-deposited layer of CBP and mCP. The device with CBP sole layer shows driving voltage of 6.36 V at 100 $mAcm^{-2}$ and maximum E.Q.E. of 1.66 %. The efficiency of device with CBP and mCP bilayer is higher than that of device with CBP sole layer but lower than that of device with CBP:mCP co-deposited layer. This result means that high performance of blue-QLED with CBP:mCP co-deposited layer is synergetic effects of electron blocking by the high LUMO energy level of HTL and higher hole density of HTL. The operational stability of the blue-QLED employing CBP:mCP co-deposited layer is improved by the enhanced device efficiency and reduced operation voltage.

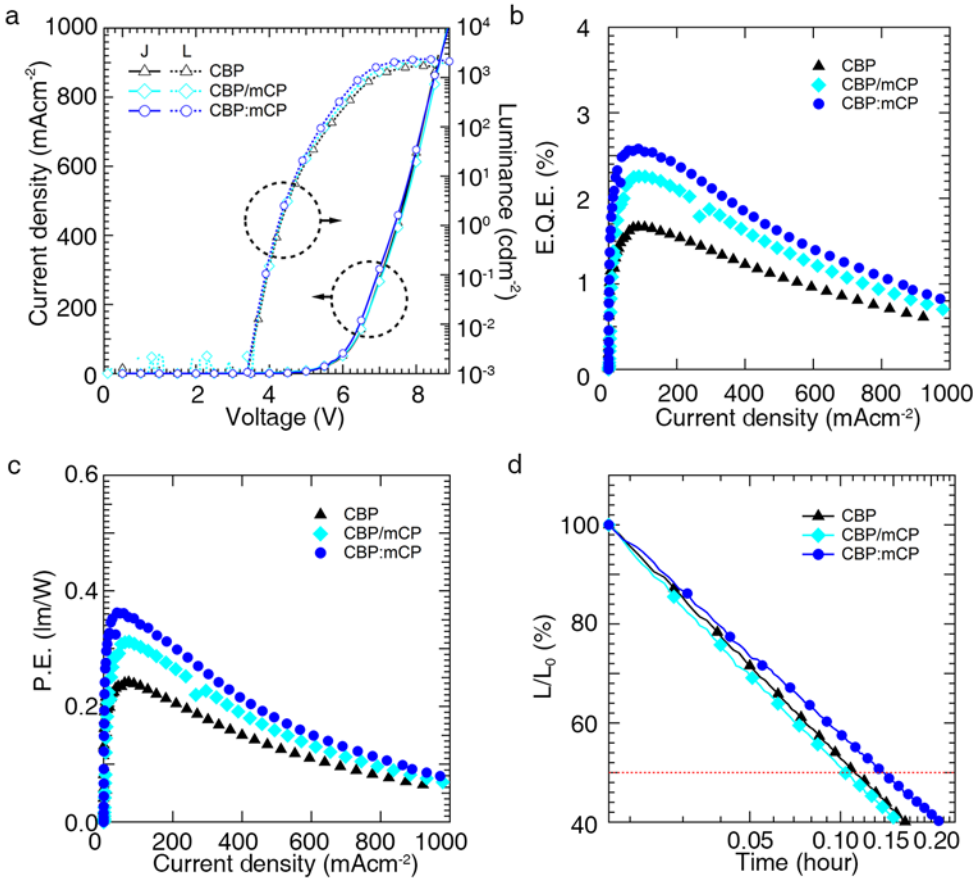

Figure 3.19 (a) *J* - *V* - *L* characteristics, (b) E.Q.E. and (c) P.E. versus *J* of blue QLEDs with CBP sole layer, CBP/mCP bilayer or CBP:mCP co-deposited layer. (d) Operational stability test results of blue QLEDs with CBP sole layer, CBP/mCP bilayer or CBP:mCP co-deposited layer. Initial luminance (L_0) of QLEDs is 200 cdm^{-2}.

3.7 Summary

In summary, we have demonstrated blue QLEDs implementing co-deposition of hole transport layer that exhibits enhanced device performance. Co-deposition layer of CBP and mCP HTL has appropriate surface energy and electronic properties to produce uniform surface on blue QD and to improve the device efficiency. In detail, we have employed CBP:mCP co-deposited layer in 1:1 volume ratio as HTL of blue QLED to obtain morphological homogeneity during device fabrication as well as suitable electronic properties ,*i.e*. hole density and LUMO energy level of HTL, to enhance hole injection rates into larger bandgap blue QDs. Local electric fields from HTL to anode are enhanced due to electron accumulation, supports efficient hole injection into larger bandgap blue QD. Higher hole density of CBP:mCP co-deposition layer also elevates hole current over devices. Increased hole current and condensed local electric field enhance hole injection rates into blue QD layer synergistically, electron-hole balance within QD emissive layer and thereby luminescence efficiency of blue QLED is improved. As a result, blue QLED with CBP:mCP co-deposited layer shows two-fold increased E.Q.E. and reduced driving voltage.

Chapter 4

White Quantum Dot Light-Emitting Diodes with Improved Efficiency and Stability Using Co-deposited Hole Transport Layer

Recent achievements of QLEDs in the research field and industrial needs for the QLED as next generation display require the research on realization of the white QLEDs accomplished by pixelation of red, green and blue QD [59, 90, 91] or mixed layer of red green and blue QD [11, 44, 92]. Among realizing methods for white QLEDs, fabricating white QLED using mixed-colored QD emissive layer is potential approach due to the simple device architecture and controllable white color

quality. As discussed in Chapter 1, overall efficiency of white-QLEDs using mixed QD emissive layer is largely affected by blue-QDs. Enhancement in the efficiency of blue-QLEDs allows small fraction of blue-QDs in red-, green- and blue-QDs mixture by increasing electroluminescence (EL) intensity positioned at blue wavelength region in the white-emission spectra. The Synergetic effects of improved device efficiency of blue-QDs and reduced portion of blue-QDs in red-, green-, and blue-mixed QDs achieve high performance of white-QLEDs. In the previous section, we proposed the blue-QLEDs implanting CBP:mCP co-deposited layer and discussed the device characteristics depending on the electrical characteristics of HTLs in terms of surface energy, hole density and LUMO energy level. As a results, we achieved two-fold enhancement in the hole injection rates and device efficiency. In this Chapter, we apply proposed architecture to white-QLEDs. Spectral changes with respect to the mixing ratio of red-, green- and blue-QDs are studied and the performance of device is investigated in terms of luminescence efficiency, color stabilities along with the operation voltage and operation time.

4.1 Characteristics of individual red, green, blue electroluminescence devices made of a co-deposited hole transport layers

The use of CBP:mCP co-deposited layer as HTL is expected to improve the hole injection rate into red and green QDs as well, and consequently the device efficiency of corresponding colored QLEDs. We have synthesized $CdSe_{1-X}S_X$(r = 1.5 nm)/ZnS(h = 6.2 nm) and CdSe(r = 2.0 nm)/$Cd_{1-X}Zn_XS$(h = 6.0 nm) core/shell type-I heterostructured QDs stabilized with oleic acids for green and red QDs, respectively (Figure 4.1). Figure 4.3 shows the device characteristics of red, green and blue QLEDs employing CBP versus CBP:mCP co-deposited layer. All red, green and blue primary color QLEDs using CBP:mCP co-deposited HTL exhibit the reduction in the driving voltage, and the improvement in the current density and the brightness (Figure 4.3a.b). Specifically, the operational voltages and the current densities at the peak E.Q.E. reduce from (5.0 V, 112.76 $mAcm^{-2}$) to (4.6 V, 102.04 $mAcm^{-2}$) for red QLED, from (5.9 V, 170.82 $mAcm^{-2}$) to (5.3 V, 120.82$mAcm^{-2}$) for green QLED, and from (5.6 V, 63.827 mAcm-2) to (5.0 V, 59.694 $mAcm^{-2}$) for blue QLED, respectively. In addition, as a result of the decrease in the driving voltage, the power efficiency and the operational stability are also enhanced in QLEDs with CBP:mCP co-deposited HTL. More specifically, red, green and blue QLEDs using CBP:mCP co-deposited layer display 0.2 V, 0.3 V and 0.7 V of reduction in the driving voltage for emitting the luminescence of 100 cdm^{-2}, and 26 %, 18 % and 7.4 % improvement in the operational lifetime, respectively (T50 refers time to reach 50 % of initial luminance under the continued operation at the fixed current density) (Figure 4.3e). These results endorse the role of CBP:mCP co-deposited HTL in the enhancement in the hole injection into QDs and the improvement of the device characteristics. We

note that the influence of the use of CBP:mCP co-deposited HTL on the device performance is less noticeable for smaller bandgap QLEDs. We attribute the reason to the diminished extent of the charge injection imbalance into relatively smaller bandgap QDs owing to the reduced energy level offset between the HOMO energy level of hole transport material and VBE energy level of smaller bandgap QDs. Figure 4.5b exhibits the Commission Internationale de l'Eclairage (CIE) 1931 color coordinates of red, green and blue QLEDs implementing CBP:mCP co-deposited layer. The combination of red, green and blue QLEDs guarantees white light with an exceptionally wide color gamut that corresponds to 150.9 % of National Television System Committee (NTSC) YR 1953 standard, 173.1 % of sRGB and 100.4 % of Rec. 2020.

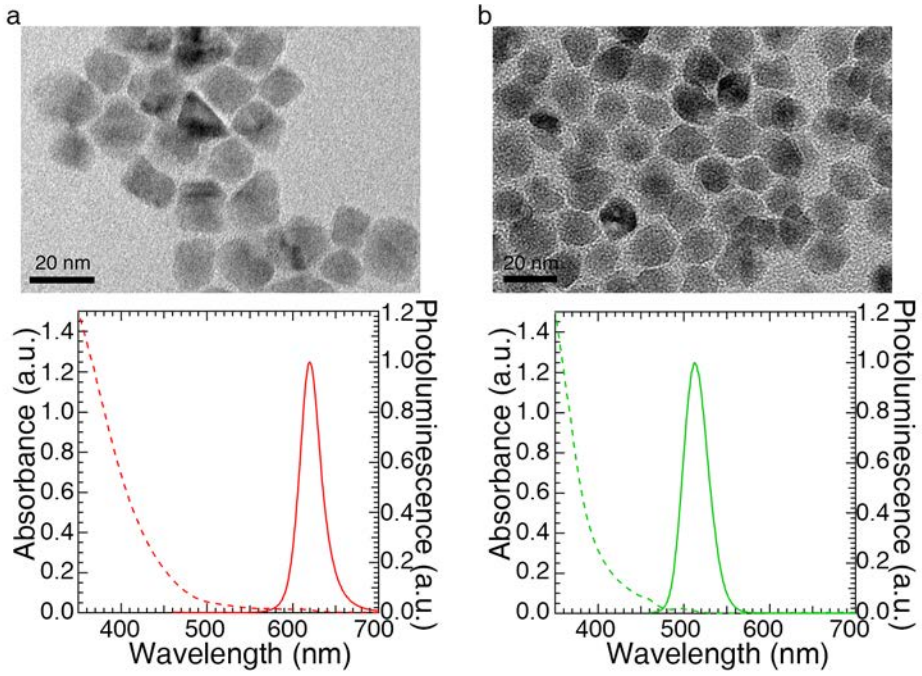

Figure 4.1 TEM images (top) and absorbance and photoluminescence spectra (bottom) of (a) CdSe(r = 2 nm)/$Cd_{1-X}Zn_XS$(h = 6.0 nm) red QDs and (b) CdSeS(r = 1.5 nm)/$Cd_{1-X}Zn_XS$(h = 6.2 nm) green QDs.

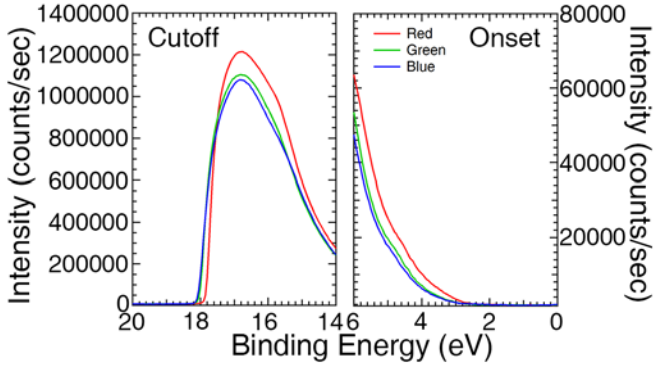

Figure 4.2 UPS spectra of red, green and blue QDs. Cutoff region (left) and onset region (right) are highlighted.

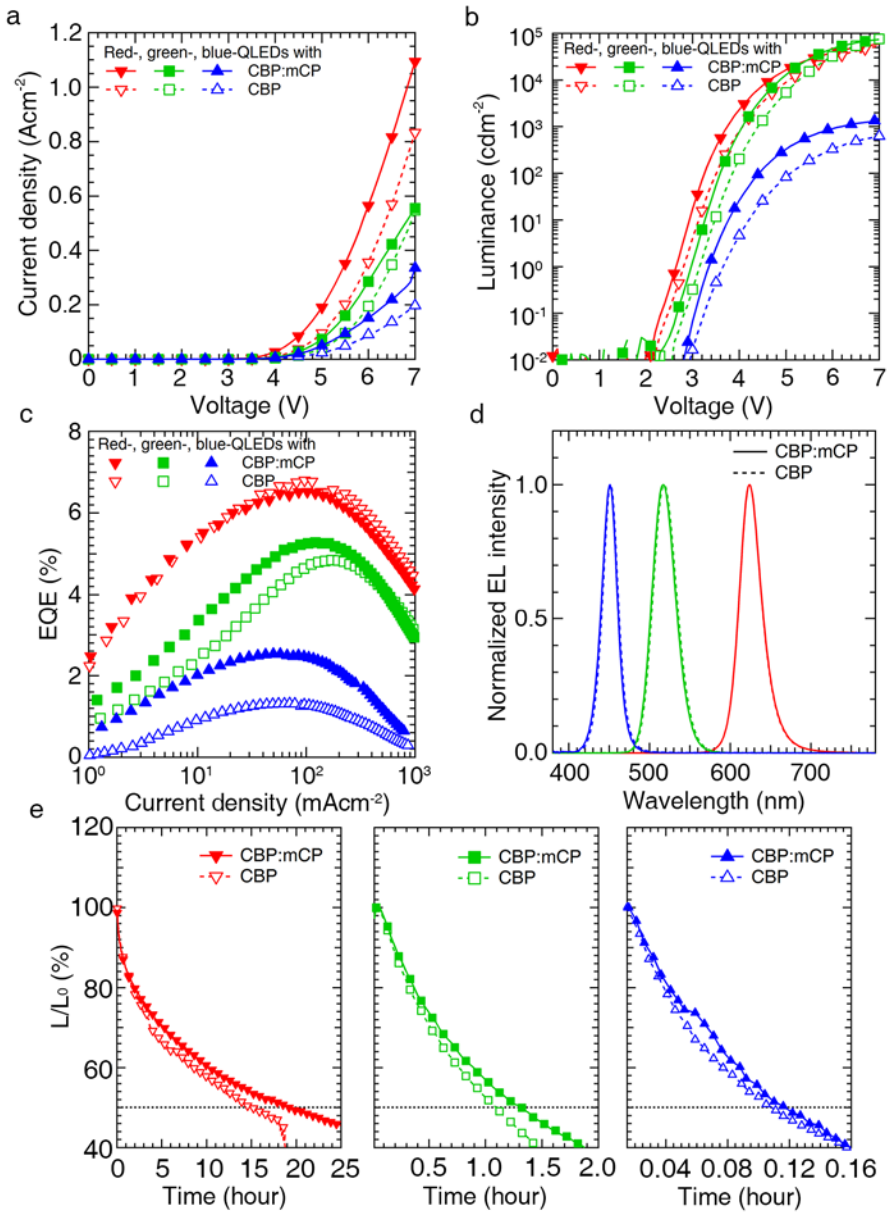

Figure 4.3 (a) *J-V*, (b) *L-V* characteristics, (c) E.Q.E. versus *J*, (d) normalized EL spectra at 50 mAcm^{-2} and (e) operational stability test results of red, green and blue QLEDs with CBP and CBP:mCP (1:1) co-deposited layer. Initial luminance (L_0) of QLEDs for the operational stability test is 1,000 cdm^{-2} for red and green QLEDs and 100 cdm^{-2} for blue QLEDs, respectively.

4.2 Characteristics of white electroluminescence devices made of a co-deposited hole transport layers

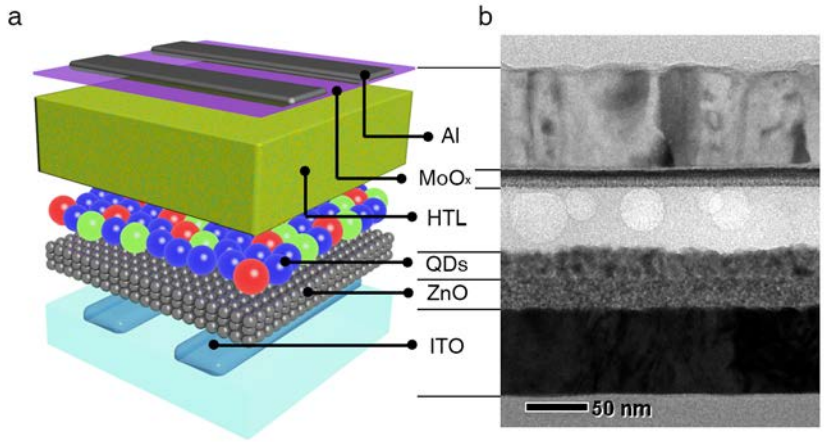

Figure 4.4 (a) Schematic illustration and (b) transmission electron microscopy (TEM) image of white QLEDs.

The excellence color purities in the color gamut along with the simplicity in the device architecture confers impetus to realize full-color white QLEDs for displays application. White QLEDs implement the emissive layer comprising red, green and blue QDs, stacked by common ZnO ETL and organic HTL (Figure 4.4) and can be understood as a parallel circuit that consists of primary color QLEDs. [11] We prepare the mixed red, green and blue QD solution in various volume ratios. White QLEDs with mixture of red, green and blue QD are fabricated using CBP:mCP co-deposited HTL and prepared solutions are spun coated as the white-emissive layer of white-QLEDs. Figure 4.5a shows the ternary phase diagram for E.Q.E. of primary color and white QLEDs. Red QLEDs exhibits highest maximum E.Q.E. value and blue QLEDs exhibits lowest maximum E.Q.E. value. The E.Q.E. of white QLEDs has relations with the mixing ratio of red, green and blue QD. As the portion of blue

QD increased, efficiency of white QLEDs go close to the blue QLEDs. In the same way, as the portion of red QD increased, E.Q.E. of device goes higher.

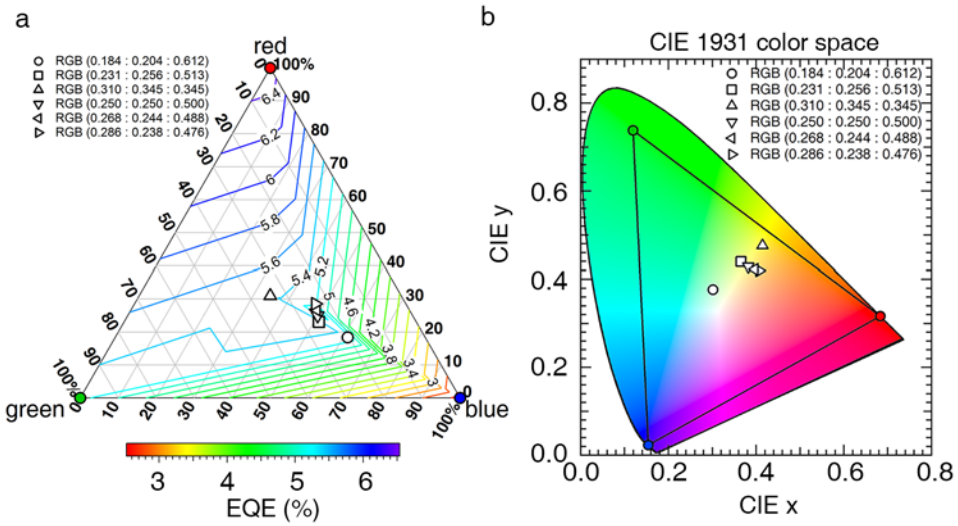

Figure 4.5 (a) Ternary phase diagram for red, green, blue and white QLEDs with CBP:mCP (1:1) codeposited layer. Devices efficiencies (*i.e.* E.Q.E.) are represented by contour and primary red, green and blue QLEDs located at each vertex. White QLEDs with 6 different mixing ratio of red, green and blue QD solution are tested. (b) CIE coordinates of white-QLEDs with 6 different mixing ratio of red, green and blue QD solution.

In this sense, we prepare the mixed red, green and blue QD solution in a volume ratio that corresponds to the inverse of E.Q.E. of primary color QLEDs (i.e., the volume ratio of red : green : blue QD solution = 0.184 : 0.204 : 0.612) to position the EL spectra of the white QLEDs close to the white point in CIE chromaticity diagram [93, 94]. Figure 4.6 present the influence of HTLs (CBP only versus CBP:mCP (1:1) co-deposited layer) on white QLED performance. As expected from primary color QLEDs, CBP:mCP co-deposited layer improves

Table 4.1 Device efficiencies (i.e. E.Q.E., P.E. and C.E.) and CIE coordinates of white QLEDs along with volume ration of red, green and blue QD solution.

Volume ratio of red, green and blue QD solution R :G : B	Max. EQE (%)	Max. PE (lmW^{-1})	Max. CE (cdA^{-1})	CIE (x, y) @1000 cdm^{-2}
0.184 : 0.204 : 0.612	5.36	6.07	9.30	(0.302, 0.377)
0.231 : 0.256 : 0.513	5.48	7.88	11.9	(0.366, 0.439)
0.310 : 0.345 : 0.345	5.46	8.40	12.30	(0.414, 0.476)
0.250 : 0.250 : 0.500	5.22	7.28	11.11	(0.382, 0.429)
0.268 : 0.244 : 0.488	5.10	7.02	10.70	(0.397, 0.422)
0.286 : 0.238 : 0.476	5.22	7.03	10.81	(0.407, 0.419)

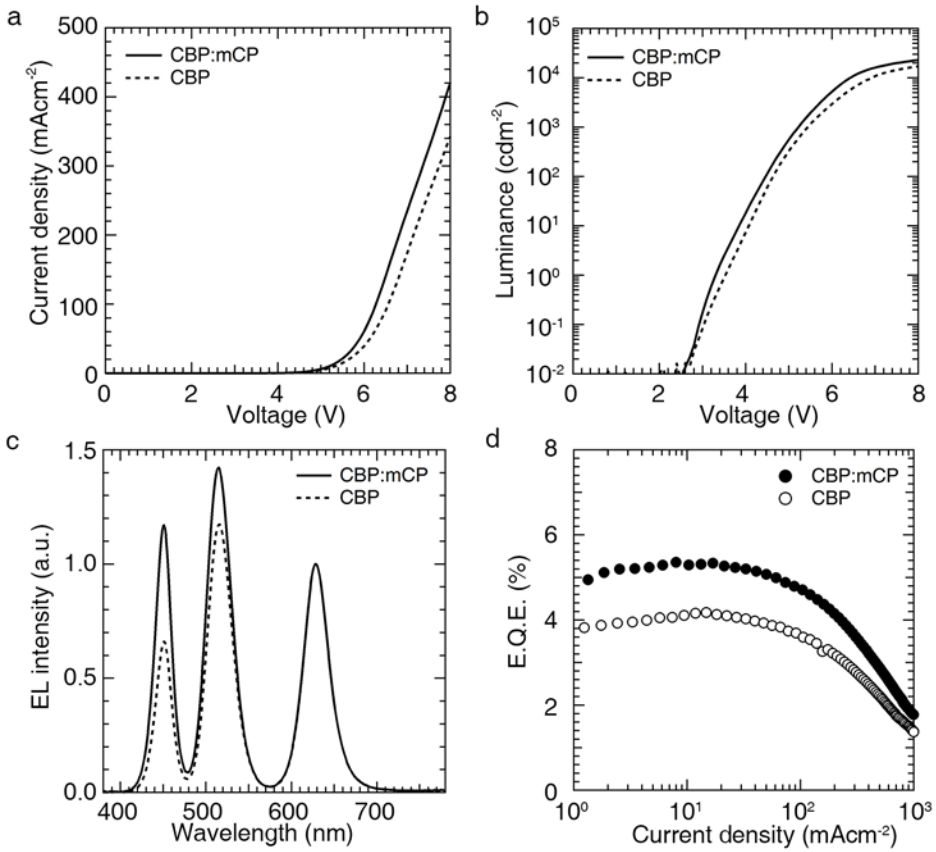

Figure 4.6 (a) *J-V* characteristic, (b) *L-V* characteristic, (c) EL spectra and (d) E.Q.E. *versus J* results of white QLEDs with CBP:mCP (1:1) co-deposited layer *versus* CBP sole layer.

the current density, the luminance and the E.Q.E. of white-QLED. Specifically, white QLED implementing CBP:mCP co-deposited layer exhibits the maximum E.Q.E. of 5.3 % and the maximum luminance of 35,527 cdm^{-2}, which is 28 % and 26 % enhancement compared to white QLED implementing CBP only. To the best of our knowledge, these are the record-high efficiency and luminance among white QLEDs displaying white-lights close to the white point in CIE chromaticity diagram. The improvement in EL intensity at higher energy regimes is more obvious (Figure

4.6c), suggesting that the improvement in the luminescence efficiency of blue and green QDs indeed leads to the increase in the E.Q.E. of white QLEDs. Due to the decrease in the driving voltage and the increase in the device efficiency, white QLED with CBP:mCP co-deposited layer requires less power (i.e. the product of current and voltage) for operation and thereby displays prolonged operational lifetime (max. T50 = 3.1 hr, average T50 = 1.19 ± 0.66 hr) compared with the case of CBP only (max. T50 = 1.4 hr, average T50 = 0.74 ± 0.26 hr) (Figure 4.7).

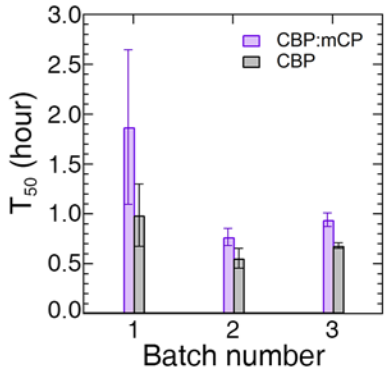

Figure 4.7 Average operation lifetime of white QLEDs from each fabrication batch. White QLEDs with CBP:mCP co-deposited layer and CBP sole layer are compared. 15 sets of white QLEDs from 3 different fabrication batches are characterized.

We note that the ratios in EL improvement in red, green and blue emission of white emission resulting from HTL engineering (0.99, 1.21 and 1.79 for red, green and blue region, respectively) agree well with E.Q.E. improvements of red, green and blue emitting primary color QLEDs (0.97, 1.21 and 1.94 for red, green and blue QLEDs) (Figure 4.6c). The similarity observed in EL spectra of white QLEDs and the E.Q.E. of primary color QLEDs falls in line with previous explanation [11] that rationalizes white QLED as a parallel circuit consisted of red, green and blue

primary color QLEDs. Minor but apparent difference detected in blue (1.79 versus 1.94) is attributed to the energy transfer from blue QDs to lower bandgap QDs within the mixed emissive layer of white QLEDs [11, 44, 59]. After optimization in the mixing ratios, we could realize white QLEDs shows the E.Q.E. of 5.36 % at the luminance of 740 cdm^{-2} and white-emissions located within the white zone over varying luminance from 100 cdm^{-2} to 10,000 cdm^{-2} (Figure 4.8).

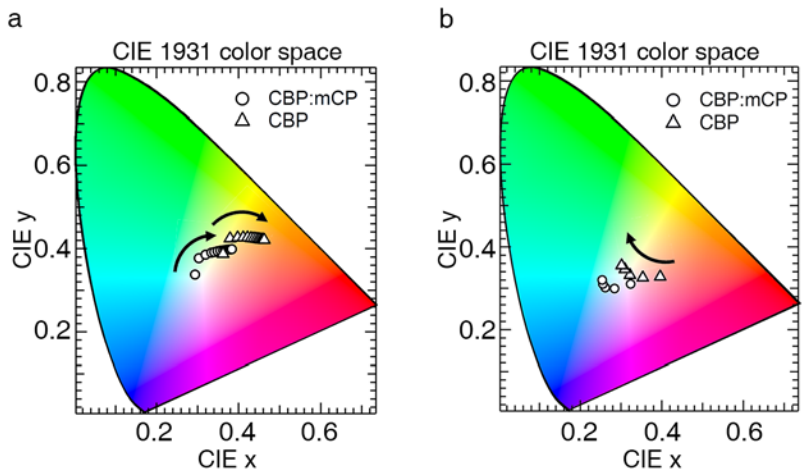

Figure 4.8 Change of the CIE 1931 *x*, *y* coordinates (a) over time and (b) over operational voltages for the EL spectra from devices with CBP:mCP (circle) and CBP (triangle). (a) CIE *x*, *y* coordinates correspond to EL spectra from the device are pointed temporal condition ranging from 0 min to 60 min in the interval of 5 min. (b) CIE *x*, *y* coordinates correspond to EL spectra from the device are pointed operational condition ranging from 4.5 V to 6.5 V in the interval of 0.5 V.

4.3 The role of co-deposited HTL on the temporal color stability of devices

To better understand the role of HTLs on the operational stability, the time-dependent changes of individual emissions (red, green and blue) from white QLEDs are inspected. We have measured EL spectra of white QLEDs on regular time basis while continuously operating devices under constant current densities (L_0 ~ 1,000 cdm^{-2}) (Figure 4.9) and decoupled red (from 570 nm to 780 nm), green (from 480 nm to 570 nm) and blue (from 380 nm to 480 nm) emission region from the white EL spectra (Figure 4.8c). Calculated initial luminance for red, green and blue region in white-emission is 287 cdm^{-2}, 736 cdm^{-2} and 28 cdm^{-2} for the device using CBP:mCP co-deposited layer, and 326 cdm^{-2}, 617 cdm^{-2} and 15 cdm^{-2} for the case using CBP only. The employment of CBP:mCP co-deposited layer increases the contribution of EL from green and blue that are less stable than the red (Figure 4.3). However, CBP:mCP co-deposited HTL improves the operation stability of all color components, particularly blue, and thus leads to the enhancement of the operational stability of white QLED (Figure 4.9c). As a result of higher initial luminance and slower decay of blue emission, white-emission from white QLEDs employing CBP:mCP co-deposited layer remains in the white zone after the luminance of devices decreases down to 50 % of initial luminance.

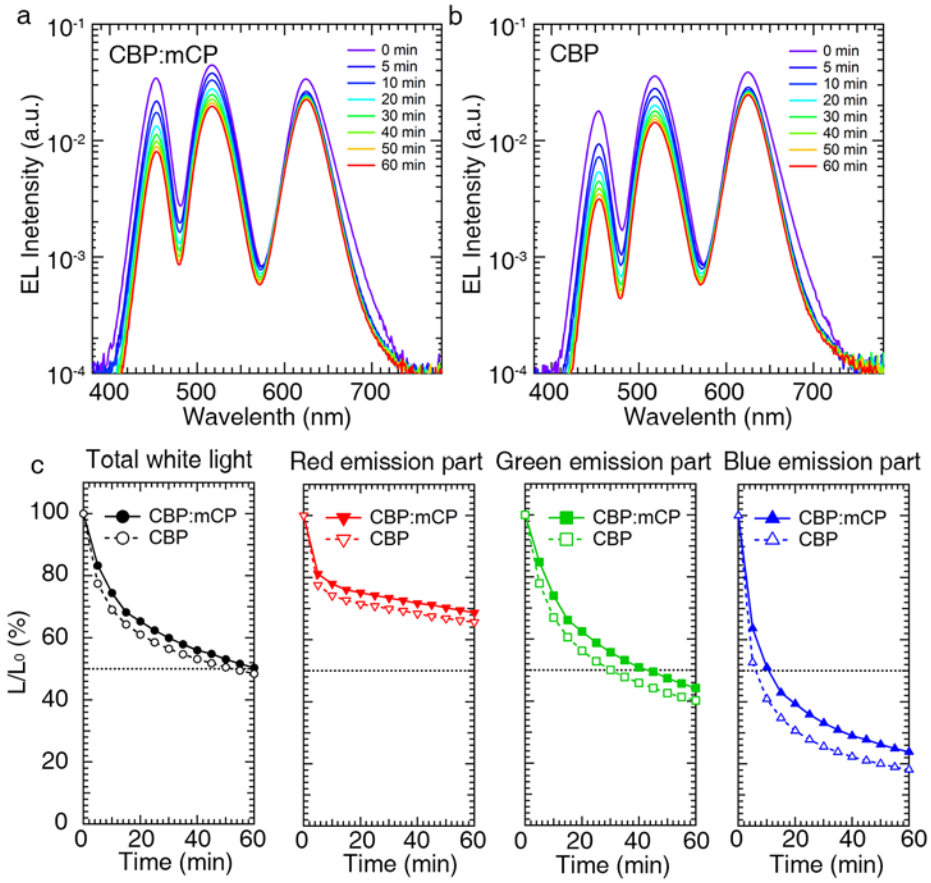

Figure 4.9 Temporal evolution of EL spectra of white QLEDs with (a) CBP:mCP (1:1) co-deposited layer and (b) CBP only. (c) Comparison of the operational stability of two devices in terms of total white light and decoupled red (570 nm – 780 nm), green (480 nm – 570 nm) and blue (380 – 480 nm) emission region from the white EL spectra. Initial luminance (L_0) is 1,051 cdm^{-2} for the white QLED with CBP:mCP and 958 cdm^{-2} for that with CBP. Decoupled L_0 for red, green and blue region in white-emission is 287 cdm^{-2}, 736 cdm^{-2} and 28 cdm^{-2} for the device with CBP:mCP co-deposited HTL, and 326 cdm^{-2}, 617 cdm-2 and 15 cdm^{-2} for the case with CBP only. The dashed guidelines indicate 50 % of the initial luminance.

4.4 The role of co-deposited HTL on the color stability of devices over varying operational conditions

Along with the improvement in the device efficiency and the temporal color-stability, the use of co-deposited HTL allows to achieve the color stability in white QLEDs over varying operation conditions. Figure 4.10 compares the spectral changes of white QLEDs employing CBP *versus* CBP:mCP co-deposited HTL over varying operation voltages (current densities or luminance). Despite large number fractions of blue and green QD (> 80 %) in the mixed QD emissive layer, their EL contribution in white QLEDs with CBP is less than 40 % at 4.5 V (70 cdm^{-2}) and below 60 % until the operational voltage is increased to 6.5 V (3,020 cdm^{-2}). Increasing the fractions of blue and green QDs enhances the color balance at the low operational voltage regime, but it results in the inevitable reduction in the device efficiency. By contrast, the use of CBP:mCP co-deposited layer enhances the color balance of white QLEDs over varying operational voltage from the same QD mixed active layer. The enhanced color balance of white-emission, particularly at the low applied voltage regime (< 5 V), is attributed to the decrease in the driving voltage of green and blue QDs that increases the exciton densities within these QDs at the low applied voltage regime. In addition, the facilitated hole injection *via* the engineered HTL helps enhance the charge balance within green and blue QDs and thereby improve their luminescence efficiency in the devices. Combined together, white QLED using CBP:mCP co-deposited HTL exhibits white-emissions with the enhanced color stability at the luminance ranging from 100 cdm^{-2} to 10,000 cdm^{-2}.

The spectral change over varying applied voltages (or current densities) is inevitable in the present device architecture, in which primary color QDs with different *J-V-L* characteristics consist of a parallel circuit. However, the results in

the present study represent that white-emissions appropriate for practicable applications, specifically, luminance ranging from 100 cdm^{-2} to 10,000 cdm^{-2} under operational voltage below 6.5 V, can be attained by means of the materials engineering. We believe that further development in materials along with the optimization of the device structure will advance the device performance in terms of the device efficiency, the operational stability and the color stability, and eventually lead us to utilize white-QLEDs in a variety of light-emitting applications.

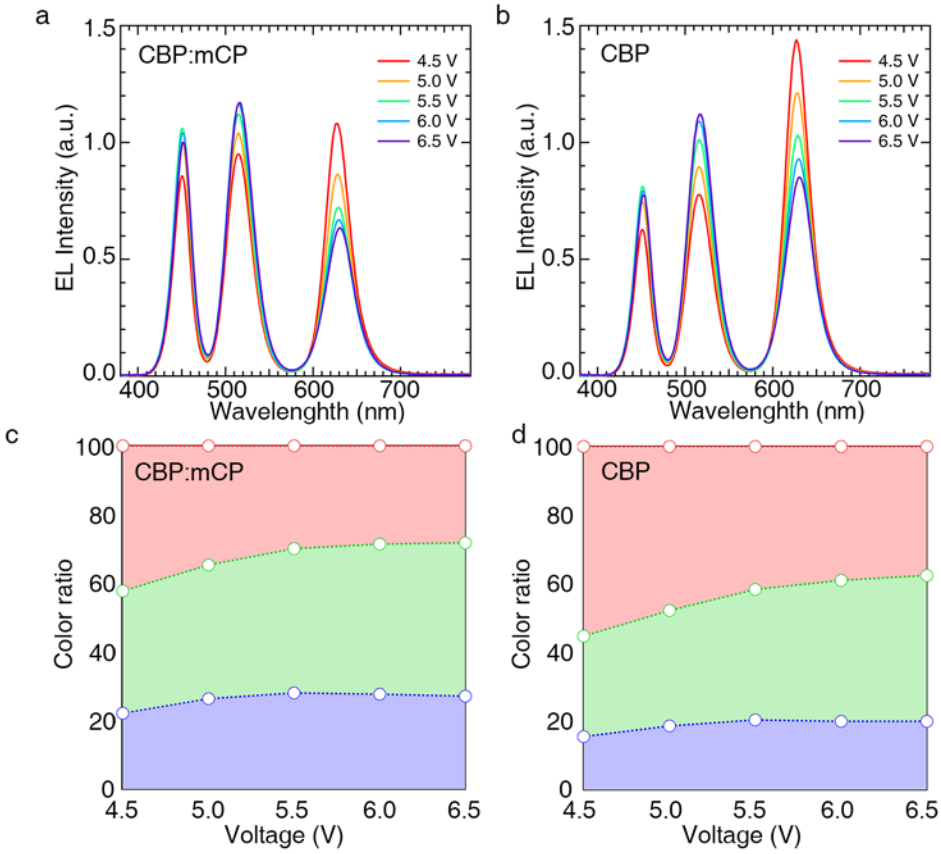

Figure 4.10 (a,b) EL spectra and (c,d) spectral color ratios of white QLEDs employing the HTL of (a,c) CBP:mCP (1:1) co-deposited layer and (b,d) CBP only layer under varying operating voltages from 4.5 V to 6.5 V. The EL spectra are normalized by the spectral area.

4.5 Summary

In summary, we have proven that engineering the electronic properties of charge transport layer can significantly improve the device performance of white QLEDs. White QLEDs implementing co-deposited hole transport layer exhibit enhanced device efficiency, operational stability and color stability. In detail, we have condensed local electric field and increased hole density in HTL to enhance the hole injection rates into larger bandgap green and blue QDs. The electron-hole balance within QD emissive layer are improved sequentially by the increased hole injection rates into larger bandgap QDs. Larger bandgap QLEDs shows the improvement in device efficiency and reduction in driving voltages. White QLEDs, regarded as the parallel circuits of primary colored QLEDs, display enhanced device efficiency, operational stability and color stability accordingly. Resulting device, white QLED employing CBP:mCP co-deposited layer in 1:1 volume ratio exhibits outstanding performance in terms of white-lights emitting close to equal energy point in CIE 1931 chromaticity diagram realized by combining of red, green and blue primary color with E.Q.E. over 5 % and color-stability at the brightness ranging from 100 to 10,000 cdm^{-2}.

Chapter 5

Conclusion

In this thesis, high performance white quantum dot light-emitting diodes based on inverted structure have been systematically studied in terms of device mechanisms and thereby device structure engineering. We demonstrated highly efficient and color-stable white quantum dot light-emitting diodes with co-deposited hole transport layer of carbazole derivatives.

First, we have demonstrated blue QLEDs implementing co-deposition of hole transport layer that exhibits enhanced device performance. Co-deposition layer of CBP and mCP HTL has appropriate surface energy and electronic properties to produce uniform surface on blue QD and to improve the device efficiency. In detail, we have employed CBP:mCP co-deposited layer in 1:1 volume ratio as HTL of blue QLED to obtain morphological homogeneity during device fabrication as well as suitable electronic properties ,*i.e*. hole density and LUMO energy level of HTL, to

enhance hole injection rates into larger bandgap blue QDs. Local electric fields from HTL to anode are enhanced due to electron accumulation, supports efficient hole injection into larger bandgap blue QD. Higher hole density of CBP:mCP co-deposition layer also elevates hole current over devices. Increased hole current and condensed local electric field enhance hole injection rates into blue QD layer synergistically, electron-hole balance within QD emissive layer and thereby luminescence efficiency of blue QLED is improved. As a result, blue QLED with CBP:mCP co-deposited layer shows two-fold increased E.Q.E. and reduced driving voltage.

CBP:mCP co-deposited layer is also applied to white QLED. Suggested device structure has proven that engineering the electronic properties of charge transport layer can significantly improve the device performance of white QLEDs. White QLEDs implementing co-deposited hole transport layer exhibit enhanced device efficiency, operational stability and color stability. In detail, we have condensed local electric field and increased hole density in HTL to enhance the hole injection rates into larger bandgap green and blue QDs. The electron-hole balance within QD emissive layer are improved sequentially by the increased hole injection rates into larger bandgap QDs. Larger bandgap QLEDs shows the improvement in device efficiency and reduction in driving voltages. White QLEDs, regarded as the parallel circuits of primary colored QLEDs, display enhanced device efficiency, operational stability and color stability accordingly. Resulting device, white QLED employing CBP:mCP co-deposited layer in 1:1 volume ratio exhibits outstanding performance in terms of white-lights emitting close to equal energy point in CIE 1931 chromaticity diagram realized by combining of red, green and blue primary color with E.Q.E. over 5 % and color-stability at the brightness ranging from 100 to 10,000 cdm^{-2}.

In conclusion, this thesis offers a technological guideline to enhance the carrier injection into larger bandgap QDs and improve device efficiency of QLEDs composed of larger bandgap QDS. We believe that approach method and designed device structure in this thesis can be useful to realize efficient and color-stable white QLEDs enough to use in real application.

Bibilography

[1] A. I. Ekimov and A. A. Onushchenko, "Quantum Size Effect in the Optical-Spectra of Semiconductor Micro-Crystals" *Sov. Phys. Semicond.* **16**, 775 (1982)

[2] R. Rossetti, S. Nakahara and L. E. Brus, "Quantum size effects in the redox potentials, resonance Raman spectra, and electronic spectra of CdS crystallites in aqueous solution" *J. Chem. Phys.* **79**, 1086 (1983)

[3] H. Woo, J. Lim, Y. Lee, J. Sung, H. Shin, J. M. Oh, M. Choi, H. Yoon, W. K. Bae and K. Char, "Robust, processable, and bright quantum dot/organosilicate hybrid films with uniform QD distribution based on thiol-containing organosilicate ligands" *J. Mater. Chem. C* **1**, 1983 (2013)

[4] L. Brus, "Electronic wave functions in semiconductor clusters: experiment and theory" *J. Phys. Chem.* **90**, 2555 (1986)

[5] A. P. Alivisatos, "Perspectives on the physical chemistry of semiconductor nanocrystals" *J. Phys. Chem.* **100**, 13226 (1996)

[6] V. I. Klimov. *Nanocrystal quantum dots*. 2nd ed. CRC Press: Boca Raton, (2010)

[7] J. H. Chang, D. Hahm, K. Char and W. K. Bae, "Interfacial engineering of core/shell heterostructured nanocrystal quantum dots for light-emitting applications" *J. Inf. Disp.* **18**, 57 (2017)

[8] W. K. Bae, S. Brovelli and V. I. Klimov, "Spectroscopic insights into the performance of quantum dot light-emitting diodes" *MRS Bulletin* **38**, 721 (2013)

[9] C. B. Murray, C. R. Kagan and M. G. Bawendi, "Synthesis and Characterization of Monodisperse Nanocrystals and Close-Packed Nanocrystal Assemblies" *Annu. Rev. Mater. Sci.* **30**, 545 (2000)

[10] P. O. Anikeeva, J. E. Halpert, M. G. Bawendi and V. Bulović, "Electroluminescence from a Mixed Red−Green−Blue Colloidal Quantum Dot Monolayer" *Nano Lett.* **7**, 2196 (2007)

[11] W. K. Bae, J. Lim, D. Lee, M. Park, H. Lee, J. Kwak, K. Char, C. Lee and S. Lee, "R/G/B/Natural White Light Thin Colloidal Quantum Dot-Based Light-Emitting Devices" *Adv. Mater.* **26**, 6387 (2014)

[12] X. Yang, Y. Divayana, D. Zhao, K. Swee Leck, F. Lu, S. Tiam Tan, A. Putu Abiyasa, Y. Zhao, H. Volkan Demir and X. Wei Sun, "A bright cadmium-free, hybrid organic/quantum dot white light-emitting diode" *Appl. Phys. Lett.* **101**, 233110 (2012)

[13]T. Zhanao, B. Hedrick, Z. Fan, Z. Ting, X. Jian, R. H. Henderson, J. Ruzyllo and A. Y. Wang, "Stable Binary Complementary White Light-Emitting Diodes Based on Quantum-Dot/Polymer-Bilayer Structures" *IEEE Photon. Technol. Lett.* **20**, 1998 (2008)

[14] E. Jang, S. Jun, H. Jang, J. Lim, B. Kim and Y. Kim, "White-Light-Emitting Diodes with Quantum Dot Color Converters for Display Backlights" *Adv. Mater.* **22**, 3076 (2010)

[15] K.-J. Chen, H.-C. Chen, K.-A. Tsai, C.-C. Lin, H.-H. Tsai, S.-H. Chien, B.-S. Cheng, Y.-J. Hsu, M.-H. Shih, C.-H. Tsai, H.-H. Shih and H.-C. Kuo, "Resonant-Enhanced Full-Color Emission of Quantum-Dot-Based Display Technology Using a Pulsed Spray Method" *Adv. Func. Mater.* **22**, 5138 (2012)

[16] S. Jun, J. Lee and E. Jang, "Highly Luminescent and Photostable Quantum Dot–Silica Monolith and Its Application to Light-Emitting Diodes" *ACS Nano* **7**, 1472 (2013)

[17] Z. Luo, Y. Chen and S.-T. Wu, "Wide color gamut LCD with a quantum dot backlight" *Opt. Express* **21**, 26269 (2013)

[18] A. J. Nozik, "Quantum dot solar cells" *Physica E: Low-dimens. syst. nanostruct.* **14**, 115 (2002)

[19] S. A. McDonald, G. Konstantatos, S. Zhang, P. W. Cyr, E. J. D. Klem, L. Levina and E. H. Sargent, "Solution-processed PbS quantum dot infrared photodetectors and photovoltaics" *Nat. Mater.* **4**, 138 (2005)

[20] J. Tang, K. W. Kemp, S. Hoogland, K. S. Jeong, H. Liu, L. Levina, M. Furukawa, X. Wang, R. Debnath, D. Cha, K. W. Chou, A. Fischer, A. Amassian, J. B. Asbury and E. H. Sargent, "Colloidal-quantum-dot photovoltaics using atomic-ligand passivation" *Nat. Mater.* **10**, 765 (2011)

[21] C. S. Erickson, L. R. Bradshaw, S. McDowall, J. D. Gilbertson, D. R. Gamelin and D. L. Patrick, "Zero-Reabsorption Doped-Nanocrystal Luminescent Solar Concentrators" *ACS Nano* **8**, 3461 (2014)

[22] J. Bomm, A. Büchtemann, A. J. Chatten, R. Bose, D. J. Farrell, N. L. A. Chan, Y. Xiao, L. H. Slooff, T. Meyer, A. Meyer, W. G. J. H. M. van Sark and R. Koole, "Fabrication and full characterization of state-of-the-art quantum dot luminescent solar concentrators" *Solar Energy Mater. Solar Cells* **95**, 2087 (2011)

[23] N. D. Bronstein, L. Li, L. Xu, Y. Yao, V. E. Ferry, A. P. Alivisatos and R. G. Nuzzo, "Luminescent Solar Concentration with Semiconductor Nanorods and Transfer-Printed Micro-Silicon Solar Cells" *ACS Nano* **8**, 44 (2014)

[24] F. Meinardi, A. Colombo, K. A. Velizhanin, R. Simonutti, M. Lorenzon, L. Beverina, R. Viswanatha, V. I. Klimov and S. Brovelli, "Large-area luminescent solar concentrators based on 'Stokes-shift-engineered' nanocrystals in a mass-polymerized PMMA matrix" *Nat. Photon.* **8**, 392 (2014)

[25] X. Michalet, "Quantum Dots for Live Cells, in Vivo Imaging, and Diagnostics" *Science* **307**, 538 (2005)

[26] U. Hasegawa, S.-i. M. Nomura, S. C. Kaul, T. Hirano and K. Akiyoshi, "Nanogel-quantum dot hybrid nanoparticles for live cell imaging" *Biochem. Biophys. Res. Commun.* **331**, 917 (2005)

[27] P. Zrazhevskiy, M. Sena and X. Gao, "Designing multifunctional quantum dots for bioimaging, detection, and drug delivery" *Chem. Soc. Rev.* **39**, 4326 (2010)

[28] V. L. Colvin, M. C. Schlamp and A. P. Alivisatos, "Light-emitting diodes made from cadmium selenide nanocrystals and a semiconducting polymer" *Nature* **370**, 354 (1994)

[29] S. Coe, W.-K. Woo, M. Bawendi and V. Bulović, "Electroluminescence from single monolayers of nanocrystals in molecular organic devices" *Nature* **420**, 800 (2002)

[30] Q. Sun, Y. A. Wang, L. S. Li, D. Wang, T. Zhu, J. Xu, C. Yang and Y. Li, "Bright, multicoloured light-emitting diodes based on quantum dots" *Nat. Photon.* **1**, 717 (2007)

[31] J. Kwak, W. K. Bae, M. Zorn, H. Woo, H. Yoon, J. Lim, S. W. Kang, S. Weber, H.-J. Butt, R. Zentel, S. Lee, K. Char and C. Lee, "Characterization of Quantum Dot/Conducting Polymer Hybrid Films and Their Application to Light-Emitting Diodes" *Adv. Mater.* **21**, 5022 (2009)

[32] W. K. Bae, J. Lim, M. Zorn, J. Kwak, Y.-S. Park, D. Lee, S. Lee, K. Char, R. Zentel and C. Lee, "Reduced efficiency roll-off in light-emitting diodes enabled by quantum dot–conducting polymer nanohybrids" *J. Mat. Chem. C* **2**, 4974 (2014)

[33]J. Kwak, W. K. Bae, D. Lee, I. Park, J. Lim, M. Park, H. Cho, H. Woo, D. Y. Yoon, K. Char, S. Lee and C. Lee, "Bright and Efficient Full-Color Colloidal Quantum Dot Light-Emitting Diodes Using an Inverted Device Structure" *Nano Lett.* **12**, 2362 (2012)

[34] S. Haubold, M. Haase, A. Kornowski and H. Weller, "Strongly luminescent InP/ZnS core-shell nanoparticles" *Chemphyschem* **2**, 331 (2001)

[35] J. Lim, W. K. Bae, D. Lee, M. K. Nam, J. Jung, C. Lee, K. Char and S. Lee, "InP@ZnSeS, Core@Composition Gradient Shell Quantum Dots with Enhanced Stability" *Chem. Mater.* **23**, 4459 (2011)

[36] J. Lim, M. Park, W. K. Bae, D. Lee, S. Lee, C. Lee and K. Char, "Highly Efficient Cadmium-Free Quantum Dot Light-Emitting Diodes Enabled by the Direct Formation of Excitons within InP@ZnSeS Quantum Dots" *ACS Nano* **7**, 9019 (2013)

[37] Y. Zhang, C. Xie, H. Su, J. Liu, S. Pickering, Y. Wang, W. W. Yu, J. Wang, Y. Wang, J.-i. Hahm, N. Dellas, S. E. Mohney and J. Xu, "Employing Heavy Metal-Free

Colloidal Quantum Dots in Solution-Processed White Light-Emitting Diodes" *Nano Lett.* **11**, 329 (2011)

[38] S. L. Castro, S. G. Bailey, R. P. Raffaelle, K. K. Banger and A. F. Hepp, "Synthesis and Characterization of Colloidal CuInS2Nanoparticles from a Molecular Single-Source Precursor" *J. Phys. Chem. B* **108**, 12429 (2004)

[39] J.-H. Kim, C.-Y. Han, K.-H. Lee, K.-S. An, W. Song, J. Kim, M. S. Oh, Y. R. Do and H. Yang, "Performance Improvement of Quantum Dot-Light-Emitting Diodes Enabled by an Alloyed ZnMgO Nanoparticle Electron Transport Layer" *Chem. Mater.* **27**, 197 (2015)

[40] D. J. Norris, N. Yao, F. T. Charnock and T. A. Kennedy, "High-Quality Manganese-Doped ZnSe Nanocrystals" *Nano Lett.* **1**, 3 (2001)

[41] N. Pradhan and X. Peng, "Efficient and Color-Tunable Mn-Doped ZnSe Nanocrystal Emitters: Control of Optical Performance via Greener Synthetic Chemistry" *J. Am. Chem. Soc.* **129**, 3339 (2007)

[42] J. Lim, B. G. Jeong, M. Park, J. K. Kim, J. M. Pietryga, Y.-S. Park, V. I. Klimov, C. Lee, D. C. Lee and W. K. Bae, "Influence of Shell Thickness on the Performance of Light-Emitting Devices Based on CdSe/Zn1-XCdXS Core/Shell Heterostructured Quantum Dots" *Adv. Mater.* **26**, 8034 (2014)

[43] W. K. Bae, Y.-S. Park, J. Lim, D. Lee, L. A. Padilha, H. McDaniel, I. Robel, C. Lee, J. M. Pietryga and V. I. Klimov, "Controlling the influence of Auger recombination on the performance of quantum-dot light-emitting diodes" *Nat. Commun.* **4**, (2013)

[44] K.-H. Lee, C.-Y. Han, H.-D. Kang, H. Ko, C. Lee, J. Lee, N. Myoung, S.-Y. Yim and H. Yang, "Highly Efficient, Color-Reproducible Full-Color Electroluminescent Devices Based on Red/Green/Blue Quantum Dot-Mixed Multilayer" *ACS Nano* **9**, 10941 (2015)

[45] Y. Yang, Y. Zheng, W. Cao, A. Titov, J. Hyvonen, J. R. Manders, J. Xue, P. H. Holloway and L. Qian, "High-efficiency light-emitting devices based on quantum dots with tailored nanostructures" *Nat. Photon.* (2015)

[46] X. Dai, Z. Zhang, Y. Jin, Y. Niu, H. Cao, X. Liang, L. Chen, J. Wang and X. Peng, "Solution-processed, high-performance light-emitting diodes based on quantum dots" *Nature* **515**, 96 (2014)

[47] B. H. Kim, M. S. Onses, J. B. Lim, S. Nam, N. Oh, H. Kim, K. J. Yu, J. W. Lee, J.-H. Kim, S.-K. Kang, C. H. Lee, J. Lee, J. H. Shin, N. H. Kim, C. Leal, M. Shim and J. A. Rogers, "High-Resolution Patterns of Quantum Dots Formed by Electrohydrodynamic Jet Printing for Light-Emitting Diodes" *Nano Lett.* **15**, 969 (2015)

[48] J. Han, D. Ko, M. Park, J. Roh, H. Jung, Y. Lee, Y. Kwon, J. Sohn, W. K. Bae, B. D. Chin and C. Lee, "Toward high-resolution, inkjet-printed, quantum dot light-emitting diodes for next-generation displays" *J. Soc. Inf. Disp.* **24**, 545 (2016)

[49] C. Jiang, Z. Zhong, B. Liu, Z. He, J. Zou, L. Wang, J. Wang, J. Peng and Y. Cao, "Coffee-Ring-Free Quantum Dot Thin Film Using Inkjet Printing from a Mixed-Solvent System on Modified ZnO Transport Layer for Light-Emitting Devices" *ACS Appl. Mater. Interfaces* **8**, 26162 (2016)

[50] Y. Fang, K. Ding, Z. Wu, H. Chen, W. Li, S. Zhao, Y. Zhang, L. Wang, J. Zhou and B. Hu, "Architectural Engineering of Nanowire Network Fine Pattern for 30 μm Wide Flexible Quantum Dot Light-Emitting Diode Application" *ACS Nano* **10**, 10023 (2016)

[51] G. Liu, X. Zhou and S. Chen, "Very Bright and Efficient Microcavity Top-Emitting Quantum Dot Light-Emitting Diodes with Ag Electrodes" *ACS Appl. Mater. Interfaces* **8**, 16768 (2016)

[52] M. Achermann, M. A. Petruska, D. D. Koleske, M. H. Crawford and V. I. Klimov, "Nanocrystal-Based Light-Emitting Diodes Utilizing High-Efficiency Nonradiative Energy Transfer for Color Conversion" *Nano Lett.* **6**, 1396 (2006)

[53] S. Nam, N. Oh, Y. Zhai and M. Shim, "High Efficiency and Optical Anisotropy in Double-Heterojunction Nanorod Light-Emitting Diodes" *ACS Nano* **9**, 878 (2015)

[54] H. S. Jang, B.-H. Kwon, H. Yang and D. Y. Jeon, "Bright three-band white light generated from CdSe/ZnSe quantum dot-assisted Sr[sub 3]SiO[sub 5]:Ce[sup 3+],Li[sup +]-

based white light-emitting diode with high color rendering index" *Appl. Phys. Lett.* **95**, 161901 (2009)

[55] M. G. Hyldahl, S. T. Bailey and B. P. Wittmershaus, "Photo-stability and performance of CdSe/ZnS quantum dots in luminescent solar concentrators" *Solar Energy* **83**, 566 (2009)

[56] L. V. Borkovska, N. O. Korsunska, V. I. Kushnirenko, T. R. Stara, V. P. Kladko and T. G. Kryshtab, "Study of thermal stability of CdSe/ZnSe quantum dot heterostructures" *Phys. Status Solidi (c)* **9**, 1768 (2012)

[57] F. Todescato, A. S. R. Chesman, A. Martucci, R. Signorini and J. J. Jasieniak, "Highly Luminescent and Temperature Stable Quantum Dot Thin Films Based on a ZnS Composite" *Chem. Mater.* **24**, 2117 (2012)

[58] H. Wang, K. S. Lee, J. H. Ryu, C. H. Hong and Y. H. Cho, "White light emitting diodes realized by using an active packaging method with CdSe/ZnS quantum dots dispersed in photosensitive epoxy resins" *Nanotechnology* **19**, 145202 (2008)

[59] T.-H. Kim, D.-Y. Chung, J. Ku, I. Song, S. Sul, D.-H. Kim, K.-S. Cho, B. L. Choi, J. Min Kim, S. Hwang and K. Kim, "Heterogeneous stacking of nanodot monolayers by dry pick-and-place transfer and its applications in quantum dot light-emitting diodes" *Nat. Commun.* **4**, 2637 (2013)

[60] A. R. Clapp, I. L. Medintz, H. T. Uyeda, B. R. Fisher, E. R. Goldman, M. G. Bawendi and H. Mattoussi, "Quantum Dot-Based Multiplexed Fluorescence Resonance Energy Transfer" *J. Am. Chem. Soc.* **127**, 18212 (2005)

[61] K. Chou and A. Dennis, "Förster Resonance Energy Transfer between Quantum Dot Donors and Quantum Dot Acceptors" *Sensors* **15**, 13288 (2015)

[62] http://www.sim4tec.com

[63] I. Robel, R. Gresback, U. Kortshagen, R. D. Schaller and V. I. Klimov, "Universal Size-Dependent Trend in Auger Recombination in Direct-Gap and Indirect-Gap Semiconductor Nanocrystals" *Phys. Rev. Lett.* **102**, (2009)

[64] V. I. Klimov, "Optical Gain and Stimulated Emission in Nanocrystal Quantum Dots" *Science* **290**, 314 (2000)

[65] H. H. Kim, S. Park, Y. Yi, D. I. Son, C. Park, D. K. Hwang and W. K. Choi, "Inverted Quantum Dot Light Emitting Diodes using Polyethylenimine ethoxylated modified ZnO" *Sci. Rep.* **5**, (2015)

[66] J. Yun, J. Kim, H.-K. Jang, K. J. Lee, J. H. Seo, B. J. Jung, G. Kim and J. Kwak, "Controlling charge balance using non-conjugated polymer interlayer in quantum dot light-emitting diodes" *Org. Electron.* **50**, 82 (2017)

[67] M. A. Hines and P. Guyot-Sionnest, "Bright UV-Blue Luminescent Colloidal ZnSe Nanocrystals" *J. Phys. Chem. B* **102**, 3655 (1998)

[68] Q. Lin, H. Shen, H. Wang, A. Wang, J. Niu, L. Qian, F. Guo and L. S. Li, "Cadmium-free quantum dots based violet light-emitting diodes: High-efficiency and brightness via optimization of organic hole transport layers" *Org. Electron.* **25**, 178 (2015)

[69] A. Wang, H. Shen, S. Zang, Q. Lin, H. Wang, L. Qian, J. Niu and L. Song Li, "Bright, efficient, and color-stable violet ZnSe-based quantum dot light-emitting diodes" *Nanoscale* **7**, 2951 (2015)

[70] W. K. Bae, K. Char, H. Hur and S. Lee, "Single-Step Synthesis of Quantum Dots with Chemical Composition Gradients" *Chem. Mater.* **20**, 531 (2008)

[71] W. K. Bae, M. K. Nam, K. Char and S. Lee, "Gram-Scale One-Pot Synthesis of Highly Luminescent Blue Emitting Cd1−xZnxS/ZnS Nanocrystals" *Chem. Mater.* **20**, 5307 (2008)

[72] M. D. Ho, D. Kim, N. Kim, S. M. Cho and H. Chae, "Polymer and Small Molecule Mixture for Organic Hole Transport Layers in Quantum Dot Light-Emitting Diodes" *ACS Appl. Mater. Interfaces* **5**, 12369 (2013)

[73] W. Ji, Y. Lv, P. Jing, H. Zhang, J. Wang, H. Zhang and J. Zhao, "Highly Efficient and Low Turn-On Voltage Quantum Dot Light-Emitting Diodes by Using a Stepwise Hole-Transport Layer" *ACS Appl. Mater. Interfaces* **7**, 15955 (2015)

[74] J. Lee, J.-I. Lee, J.-W. Lee and H. Y. Chu, "Effects of charge balance on device performances in deep blue phosphorescent organic light-emitting diodes" *Org. Electron.* **11**, 1159 (2010)

[75] C. Kulshreshtha, J. W. Choi, J.-k. Kim, W. S. Jeon, M. C. Suh, Y. Park and J. H. Kwon, "Open-circuit voltage dependency on hole-extraction layers in planar heterojunction organic solar cells" *Appl. Phys. Lett.* **99**, 023308 (2011)

[76] Y. Shirota and H. Kageyama, "Charge carrier transporting molecular materials and their applications in devices" *Chem. Rev.* **107**, 953 (2007)

[77] Y. Kuwabara, H. Ogawa, H. Inada, N. Noma and Y. Shirota, "Thermally stable multilared organic electroluminescent devices using novel starburst molecules, 4,4´,4˝-Tri(N-carbazolyl)triphenylamine (TCTA) and 4,4´,4˝-Tris(3-methylphenylphenylamino)triphenylamine (m-MTDATA), as hole-transport materials" *Adv. Mater.* **6**, 677 (1994)

[78] S.-C. Dong, C.-H. Gao, X.-D. Yuan, L.-S. Cui, Z.-Q. Jiang, S.-T. Lee and L.-S. Liao, "Novel dibenzothiophene based host materials incorporating spirobifluorene for high-efficiency white phosphorescent organic light-emitting diodes" *Org. Electron.* **14**, 902 (2013)

[79] Z. Q. Gao, B. X. Mi, H. L. Tam, K. W. Cheah, C. H. Chen, M. S. Wong, S. T. Lee and C. S. Lee, "High Efficiency and Small Roll-Off Electrophosphorescence from a New Iridium Complex with Well-Matched Energy Levels" *Adv. Mater.* **20**, 774 (2008)

[80] I. G. Hill and A. Kahn, "Organic semiconductor heterointerfaces containing bathocuproine" *J. Appl. Phys.* **86**, 4515 (1999)

[81] T. Tsuboi, S.-W. Liu, M.-F. Wu and C.-T. Chen, "Spectroscopic and electrical characteristics of highly efficient tetraphenylsilane-carbazole organic compound as host material for blue organic light emitting diodes" *Org. Electron.* **10**, 1372 (2009)

[82]M. F. Wu, S. J. Yeh, C. T. Chen, H. Murayama, T. Tsuboi, W. S. Li, I. Chao, S. W. Liu and J. K. Wang, "The Quest for High-Performance Host Materials for Electrophosphorescent Blue Dopants" *Adv. Func. Mater.* **17**, 1887 (2007)

[83] H. Cho, J. Kwak, J. Lim, M. Park, D. Lee, W. K. Bae, Y. S. Kim, K. Char, S. Lee and C. Lee, "Soft Contact Transplanted Nanocrystal Quantum Dots for Light-Emitting Diodes: Effect of Surface Energy on Device Performance" *ACS Appl. Mater. Interfaces* **7**, 10828 (2015)

[84] L.-W. Chong, Y.-L. Lee and T.-C. Wen, "Surface modification of indium tin oxide anodes by self-assembly monolayers: Effects on interfacial morphology and charge injection in organic light-emitting diodes" *Thin Solid Films* **515**, 2833 (2007)

[85] N. Matsusue, Y. Suzuki and H. Naito, "Charge carrier transport in neat thin films of phosphorescent iridium complexes" *Jpn. J. Appl. Phys. 1* **44**, 3691 (2005)

[86] S.-B. Lee, T. Yasuda, M.-J. Yang, K. Fujita and T. Tsutsui, "Charge Carrier Mobility in Vacuum-Sublimed Dye Films for Light-Emitting Diodes Studied by the Time-of-Flight Technique" *Mol. Cryst. Liq. Cryst.* **405**, 67 (2003)

[87] A. Armin, G. Juska, M. Ullah, M. Velusamy, P. L. Burn, P. Meredith and A. Pivrikas, "Balanced Carrier Mobilities: Not a Necessary Condition for High-Efficiency Thin Organic Solar Cells as Determined by MIS-CELIV" *Adv. Energy Mater.* **4**, 1300954 (2014)

[88] D. Y. Kondakov, "Role of chemical reactions of arylamine hole transport materials in operational degradation of organic light-emitting diodes" *J. Appl. Phys.* **104**, 084520 (2008)

[89] B. Ruhstaller, S. A. Carter, S. Barth, H. Riel, W. Riess and J. C. Scott, "Transient and steady-state behavior of space charges in multilayer organic light-emitting diodes" *J. Appl. Phys.* **89**, 4575 (2001)

[90] A. Rizzo, M. Mazzeo, M. Biasiucci, R. Cingolani and G. Gigli, "White electroluminescence from a microcontact-printing-deposited CdSe/ZnS colloidal quantum-dot monolayer" *Small* **4**, 2143 (2008)

[91] M. K. Choi, J. Yang, K. Kang, D. C. Kim, C. Choi, C. Park, S. J. Kim, S. I. Chae, T.-H. Kim, J. H. Kim, T. Hyeon and D.-H. Kim, "Wearable red–green–blue quantum dot light-emitting diode array using high-resolution intaglio transfer printing" *Nat. Commun.* **6**, 7149 (2015)

[92] X. Yang, D. Zhao, K. S. Leck, S. T. Tan, Y. X. Tang, J. Zhao, H. V. Demir and X. W. Sun, "Full Visible Range Covering InP/ZnS Nanocrystals with High Photometric Performance and Their Application to White Quantum Dot Light-Emitting Diodes" *Adv. Mater.* **24**, 4180 (2012)

[93] F. Li, W.-N. Li, S.-Y. Fu and H.-M. Xiao, "Formulating CdSe quantum dots for white light-emitting diodes with high color rendering index" *J. Alloys Compound.* **647**, 837 (2015)

[94] K. T. Kamtekar, A. P. Monkman and M. R. Bryce, "Recent Advances in White Organic Light-Emitting Materials and Devices (WOLEDs)" *Adv. Mater.* **22**, 572 (2010)

Publication

[1] International Journals

1. I. Cho*, **H. Jung***, B. G. Jeong, J. H. Chang, Y. Kim, K. Char, D. C. Lee, C. Lee, J. Cho and W. K. Bae, "Multifunctional Dendrimer Ligands for High-Efficiency, Solution-Processed Quantum Dot Light-Emitting Diodes", *ACS Nano* **11**, 684 (2017) (*:co-first).

2. J. Kim, **H. Jung**, J. Song, K. Kim and C. Lee, "Analysis of Interfacial Layer-Induced Open-Circuit Voltage Burn-In Loss in Polymer Solar Cells on the Basis of Electroluminescence and Impedance Spectroscopy" *ACS Appl. Mater. Interface*. **9**, 24052 (2017).

3. J. Son, H.-T. Oh, O J. Kwon, **H. Jung**, J.-M. Lim, B. J. Jung, D.-H. Hwang, C. Lee, J.-K. Lee, J. G. Yoon and S. Y. Yoon , "Highly Soluble Fluorous Alkyl Ether-tagged Imaging Materials for the Photo-patterning of Organic Light-Emitting Devices", *J. Mater. Chem. C* **5**, 926 (2017).

4. J. Han, D. Ko, M. Park, J. Roh, **H. Jung**, Y. Kwon, Y. Lee, J. Sohn, W. K. Bae, B. D. Chin and C. Lee, "Toward high-resolution, inkjet-printed, quantum dot

light-emitting diodes for next-generation displays", *J. Soc. Inform. Display* **24**, 545 (2016).

5. H.-J. Park, **H. Jung**, S.-H. Kim, M. Park, J.-H. Kim, J. Son, B. J. Jung, D.-H. Hwang, C. Lee, J.-K. Lee, J. G. Yoon and S. Y. Yoon, "Fluorous solvent-soluble imaging materials containing anthracene moieties", J. Poly. Sci. A: Poly. Chem. **53**, 1252 (2015).

6. M. Park, S.-H. Jung, J. Lim, D.-Y. Kim, H.-J. Kim, S. Lee, **H. Jung**, S. Lee, C. Lee and J.-K. Lee, "Semiconductor Nanocrystals in Fluorous Liquids for the Construction of Light-Emitting Diodes", J. Mater. Chem. C **3**, 2759 (2015).

7. H. Lee, Y. Kwon, **H. Jung**, J.-I. Lee and C. Lee, "Enhanced performances in inverted bottom-emission organic light-emitting diodes with KBH4-doped electron-injection layer", Phys. Status Solidi A **211**, 1807 (2014).

[2] International Conferences

1. **H. Jung**, I. Cho, B. G. Jeong, D. C. Lee, J. Cho, W. K. Bae and C. Lee, "Improved Performance of Quantum Dot Light-Emitting Diodes by Ligand Exchange of Quantum Dots", *Materials Research Society (MRS) Spring meeting*, Phoenix, USA (2017) (oral).

2. **H. Jung**, M. Park, Y. Lee, W. K. Bae and C. Lee, "Efficiency Improvement of Blue Quantum Dot Light-Emitting Diodes through Enhanced Charge Balance", *The 9th International Conference on Quantum Dots*, Jeju, Korea (2016) (poster).

3. **H. Jung**, M. Park, Y. Lee, B. G. Jeong, W. K. Bae and C. Lee, "Bright and

Efficient Blue Quantum Dot Light-Emitting Diodes with Mixed Hole Transport Layer", *Materials Research Society (MRS) Spring meeting*, Phoenix, USA (2016) (oral).

4. **H. Jung**, M. Park, Y. Lee, W. K. Bae and C. Lee, "White Quantum Dot Light-Emitting Diodes with Improved Performance Using Conjugated Polyelectrolyte, *The 15th International Meeting on Information Display (IMID)*, Daegu, Korea (2015) (poster: IMID 2015 Best poster award).

5. **H. Jung**, S.-Y. Lee, S. Jung, M. Park, Y. You, J.-K. Lee and C. Lee, "Highly Fluorinated Phosphorescent Emitter for Solution Processed Organic Light-Emitting Diodes", *2015 MRS Spring Meeting & Exhibit*, San Francisco, USA (2015) (poster).

6. **H. Jung**, M. Thambidurai, J. Lim, K. Char, S. Lee and C. Lee, "Enhanced Efficiency of Quantum Dot Light-Emitting Diodes by Modifying Sol-Gel Based Metal-doped ZnO Electron Transport Layer", 2014 *International Display Workshops*, niigata, Japan (2014) (oral).

7. **H. Jung**, M. Park, M. Thambidurai, J. Lim, J. Kwak, K. Char, S. Lee and C. Lee, "Improved Efficiency of Inverted Quantum Dot Light-Emitting Diodes Using Sol-Gel based Metal-doped ZnO as an Electron Transport Layer", *The 14th International Meeting on Information Display (IMID)*, Daegu, Korea (2014) (poster).

8. **H. Jung**, M. Park, M. Thambidurai, J. Lim, J. Kwak, K. Char, S. Lee and C. Lee, "Effect of Annealing Temperatures of Sol-Gel Based Ga-doped ZnO Electron Transport Layer on Quantum Dot Light-Emitting Diodes", *Materials Research Society (MRS) Fall Meeting*, Boston, USA (2013) (poster).

[3] Domestic Conferences

1. **H. Jung**, K. Kim, W. K. Bae and C. Lee, “Enhanced Efficiency of Blue Quantum Dot Light-Emitting Diodes by Modifying Hole Transport Layer”, *한국전기전자재료학회 2016년도 하계학술대회*, 경주 (2016) (oral).

한글 초록

콜로이드성 양자점은 광소자에 사용하기에 적합한 광학적 전기적 특성을 가지고 있다. 그중에서도 양자점은 높은 양자효율, 넓은 흡수 파장대와 좁은 발광 파장대, 열안정성과 광안정성을 가지고 있기 때문에 발광다이오드의 광물질로 사용하기에 적합하다. 다년간의 소재에 대한 개발과 소자 구조에 대한 연구를 통하여 양자점 발광다이오드는 소자 특성과 구조적으로 많은 발전이 있어 왔다. 양자점 발광다이오드의 다양한 응용중에서 백색 발광 양자점 발광다이오드는 단순한 소자구조를 가지고 있는 점, 그러면서도 백색 파장을 자유롭게 조절할 수 있다는 점에서 큰 매력을 가지고 있다. 그러나 큰 밴드갭을 가지는 청색양자점은 양자점 발광다이오드의 전하 주입 불균일을 야기하고 이는 고효율 백색 양자점 발광다이오드를 구현하는데 큰 제한이 된다. 본 논문에서는 정공수송층의 개발을 통하여 밴드갭이 큰 양자점으로의 정공주입속도를 제어하여 소자의 특성을 향상시키고 최종적으로 높은 효유과 색 안정성을 가지고 있는 백색 양자점 발광다이오드의 구현하였다.

먼저 정공수송층 개발을 통한 밴드갭이 큰 청색 양자점 발광다이오드의 특성을 향상시키는 연구가 진행되었다. 최고준위점유분자궤도 (HOMO, Highest occupied molecular orbital) 에너지 준위와 청색 양자점 발광다이오드의 소자 특성상과의 상관관계가 연구되었다. CBP, mCP, TCTA, TAPC, NPB 정공수송층을 소자에 적용하여 HOMO 에너지 준위와 소자 성능과의 관계가 분석되었고, 이를 통하여 고성능 소자를 구현하기 위한 정공수송층 물질로 CBP 와 mCP 가 채택되었다. 양자점과 정공수송층과의 표면에너지 차이로 인하여 mCP 가 양자점 위에 불균일하게 증착되는 현상이 발견되었고, CBP 와 mCP 의 동시 증착을 통하여 이를 해결하였다. 또한 CBP 와 mCP 가 동시증착 된

정공수송층은 밴드갭이 큰 청색 양자점에 정공을 효율적으로 주입시켰으며 이를 통하여 청색 양자점 발광다이오드의 소자효율을 두배로 증가시킬 수 있었다.

나아가 백색 양자점 발광다이오드에 대한 연구도 진행하였다. 적색, 녹색, 청색 발광다이오드가 CBP 단독 HTL 과 CBP:mCP 동시 증착 HTL 을 이용하여 각각 제작 및 분석되었다. 적색, 녹색, 청색 양자점의 혼합 비율에 따른 소자효율 변화와 스펙트럼 변화 역시 분석하였다. CBP:mCP 동시 증착 HTL 을 적용한 삼색 양자점 발광다이오드는 효율적인 정공주입으로 인하여 소자 효율과 수자 수명이 각각 증가되었다. 소자 특성 향상폭은 양자점의 밴드갭이 클수록 증가되었으며 밴드갭이 가장 큰 청색 양자점의 소자 성능이 가장 큰 폭으로 증가하였다. 또한 청색 양자점 발광다이오드의 구동전압이 가장 큰 폭으로 감소하였기 때문에 적색, 녹색, 청색 양자점을 혼합한 백색 양자점 발광다이오드의 구동전압에 따른 색 변화율이 큰 폭으로 감소하였다. 그 결과 소자 휘도 100 cdm^{-2} 에서 10,000 cm^{-2} 구간에서 CIE (Commision International de l'Eclairage) 좌표상에서 백색에 위치하고 외부양자효율 5 % 이상을 유지하는 백색 양아점 발광다이오드를 구현하였다.

본 논문에서 개발된 접근 방법과 소자구조는 미래에 높은 효율과 색안정성을 가지는 백색 양자점 발광다이오드의 연구와 이를 통한 디스플레이 제품 개발에 도움이 될 것이라고 생각한다.

주요어: 양자점, 발광다이오드, 역구조, 동시 증착, 정공 수송층, 균형 전하 주입

학번: 2012-20866